

SUPPORTING INFORMATION FOR

**2-Mercaptomethyl-thiazolidines use conserved aromatic-S interactions to achieve broad-range inhibition of metallo- $\beta$ -lactamases**

Maria-Agustina Rossi<sup>a,†</sup>, Veronica Martinez<sup>b,†</sup>, Philip Hinchliffe<sup>c,†</sup>, Maria F. Mojica<sup>d,e,f</sup>, Valerie Castillo<sup>b</sup>, Diego M. Moreno<sup>g,j</sup>, Ryan Smith<sup>c</sup>, Brad Spellberg<sup>h</sup>, George L. Drusano<sup>i</sup>, Claudia Banchio<sup>a,j</sup>, Robert A. Bonomo<sup>e,k,l,m</sup>, James Spencer<sup>c</sup>, Alejandro J. Vila<sup>a,j\*</sup> and Graciela Mahler<sup>b\*</sup>

<sup>a</sup> Instituto de Biología Molecular y Celular de Rosario (IBR, CONICET-UNR), Ocampo and Esmeralda, S2002LRK Rosario, Argentina.

<sup>b</sup> Laboratorio de Química Farmacéutica, Departamento de Química Orgánica, Facultad de Química, Avda. General Flores 2124, CC1157, Universidad de la República (UdelaR), Montevideo, Uruguay

<sup>c</sup> School of Cellular and Molecular Medicine, University of Bristol, Biomedical Sciences Building, University Walk, Bristol BS8 1TD, U.K.

<sup>d</sup> Infectious Diseases Department, School of Medicine, Case Western Reserve University, Cleveland, OH, USA.

<sup>e</sup> Research Service, Louis Stokes Cleveland Department of Veterans Affairs Medical Center, Cleveland, OH, USA.

<sup>f</sup> Grupo de Resistencia Antimicrobiana y Epidemiología Hospitalaria, Universidad El Bosque, Bogotá, DC, Colombia.

<sup>g</sup> Instituto de Química de Rosario (IQUIR, CONICET-UNR), Suipacha 570, S2002LRK Rosario, Argentina.

<sup>h</sup> Los Angeles County and University of Southern California (LAC+USC) Medical Center, Los Angeles, CA, USA.

<sup>i</sup> Center for Pharmacometrics and Systems Pharmacology, Department of Pharmaceutics, College of Pharmacy, University of Florida, Orlando, FL, USA.

<sup>j</sup> Facultad de Ciencias Bioquímicas y Farmacéuticas, Universidad Nacional de Rosario, S2002LRK Rosario, Argentina

<sup>k</sup> Departments of Medicine, Pharmacology, Molecular Biology and Microbiology, Biochemistry, and Proteomics and Bioinformatics, Case Western Reserve University School of Medicine, Cleveland, OH, USA.

<sup>l</sup> Medical Service and GRECC, Louis Stokes Cleveland Department of Veterans Affairs Medical Center, Cleveland, OH, USA.

<sup>m</sup> CWRU-Cleveland VAMC Center for Antimicrobial Resistance and Epidemiology (Case VA CARES), Cleveland, OH, USA.

\* Corresponding authors: [vila@ibr-conicet.gov.ar](mailto:vila@ibr-conicet.gov.ar) and [gmahler@fq.edu.uy](mailto:gmahler@fq.edu.uy).

## TABLE OF CONTENTS

<b>Tables</b>	<b>3</b>
Table S1. Data collection and refinement statistics.	3
Table S2. Inhibitor RSCCs calculated by the PDB	4
Table S3. Interaction distances (Å) of thiazolidine inhibitors in B1 MBLs.	5
<b>Figures</b>	<b>6</b>
Figure S1. Remaining D- <i>anti</i> -1b vs time in PBS pH 7.2 at 27°C.	6
Figure S2. Chromatogram on LCMS of D- <i>anti</i> -1b after 6 h incubation in PBS pH 7.2, at 27°C.	7
Figure S3. Determination of the inhibition constant of MMTZ against the MBLs: NDM-1, VIM-2, and IMP-1.	8
Figure S4. Reaction curves of imipenem hydrolysis by NDM-1, VIM-2 and IMP-1 at different concentrations of the MMTZ inhibitors.	9
Figure S5. Imipenem hydrolysis by <i>E. coli</i> -NDM-1.	10
Figure S6. <i>In-cell</i> IC <sub>50</sub> .	11
Figure S7. Omit electron density maps of MMTZs bound in the active site of B1 MBLs.	12
Figure S8. Comparisons of MMTZ binding modes to B1 MBLs	13
Figure S9. Comparisons of MMTZ and MMOZ binding modes to NDM-1.	14
Figure S10. Comparisons of L- and D- stereoisomers of MMTZ and captopril bound in the active sites of B1 MBLs.	15
Figure S11. MMTZ and BTZ binding to IMP-1.	16
Figure S12. Comparisons of the binding modes of MMTZ and hydrolyzed antibiotic products in NDM-1.	17
Figure S13. Cell viability of <i>E. coli</i> expressing NDM-1 before and after the NMR experiments.	18
Figure S14. Imipenem stability and hydrolysis	19
<b><sup>1</sup>H, <sup>13</sup>C NMR Spectra of the MMTZ inhibitors</b>	<b>20</b>
<b>Crystal data and structure refinement of L-<i>anti</i>-1a</b>	<b>29</b>
Figure S15: ORTEP.	29
Table S4. Sample and crystal data.	30
Table S5. Data collection and structure refinement.	30
Table S6. Hydrogen bond distances (Å) and angles (°) for L- <i>anti</i> -1a.	31
<b>HPLC Purity.</b>	<b>32</b>
Figure S16: Chromatogram of compound L- <i>anti</i> -1a, monitored at 215 nm	32
Figure S17: Chromatogram of compound D- <i>anti</i> -1a, monitored at 215 nm	33
Figure S18: Chromatogram of compound L- <i>anti</i> -1b, monitored at 215 nm	33
Figure S19: Chromatogram of compound D- <i>anti</i> -1b, monitored at 215 nm	34
Figure S20: Chromatogram of compound L- <i>syn</i> -1b, monitored at 215 nm	34
Figure S21: Chromatogram of compound D- <i>syn</i> -1b, monitored at 215 nm	35
<b>Experimental Methods</b>	<b>36</b>
Chemical Stability of D- <i>anti</i> -1b	36
LCMS/MS chromatogram	36
Protein preparation for K <sub>i</sub> determinations	36
Determination of the K <sub>i</sub> .	36
Bacterial cell preparations for inhibition studies	37
<sup>1</sup> H NMR measurements and analyses	37
<i>In-cell</i> IC <sub>50</sub> measurements and analyses	37
Antimicrobial susceptibility testing	37
Cell Culture and Survival Assay	38
Crystallization and Structure Determination	38
QM-MM calculations	38
<b>References</b>	<b>39</b>

## Tables

**Table S1. Data collection and refinement statistics.**

Inhibitor	VIM-2		NDM-1		IMP-1	
	L- <i>anti-1b</i>	D- <i>syn-1b</i>	L- <i>anti-1b</i>	D- <i>syn-1b</i>	L- <i>anti-1b</i>	D- <i>syn-1b</i>
PDB accession	6zyn	6zyo	6zyp	6zyq	6zyr	6zys
<b>Data collection</b>						
Space group	I2	C2	P212121	P212121	P212121	P212121
Molecules/ASU	2	2	2	2	4	4
Cell dimensions						
a, b, c (Å)	67.48, 79.17, 78.07	103.56, 79.74, 68.04	69.97, 74.18, 77.96	70.18, 73.84, 77.44	48.56, 78.00, 261.11	48.78, 77.97, 261.91
$\alpha$ , $\beta$ , $\gamma$ (°)	90.0, 90.5, 90.0	90.0, 130.5, 90.0	90.0, 90.0, 90.0	90.0, 90.0, 90.0	90.0, 90.0, 90.0	90.0, 90.0, 90.0
Wavelength	0.91588	0.91587	0.97634	0.97629	0.91588	0.97949
Resolution (Å)	55.59 – 1.40 (1.42 – 1.40)	51.76 – 1.45 (1.48 – 1.45)	53.74 – 1.40 (1.42 – 1.40)	38.72 – 1.70 (1.74 – 1.70)	66.96 – 1.87 (1.91 – 1.87)	58.15 – 1.87 (1.91 – 1.87)
R <sub>pim</sub>	0.077 (0.357)	0.027 (0.497)	0.039 (0.344)	0.031 (0.596)	0.053 (0.410)	0.026 (0.469)
CC 1/2	0.986 (0.567)	0.999 (0.675)	0.997 (0.584)	0.999 (0.473)	0.998 (0.542)	0.999 (0.784)
I / $\sigma$ I	4.8 (2.0)	16.8 (1.6)	11.1 (2.4)	13.1 (1.2)	9.4 (2.1)	18.6 (1.8)
Completeness (%)	99.7 (99.7)	98.7 (97.5)	99.0 (94.1)	99.5 (94.2)	100.0 (100.0)	100.0 (100.0)
Redundancy	5.1 (5.0)	6.8 (7.0)	12.3 (9.3)	12.2 (8.3)	13.0 (13.6)	26.2 (26.5)
<b>Refinement</b>						
Resolution (Å)	55.59 – 1.40	54.76 – 1.45	42.62 – 1.40	38.72 – 1.70	66.96 – 1.87	58.15 – 1.87
No. reflections	80183	73389	79559	44721	83159	83742
R <sub>work</sub> / R <sub>free</sub>	14.97 / 17.62	12.42 / 16.33	16.35 / 18.73	17.75 / 19.76	18.30 / 21.87	17.41 / 20.13
No. non-H atoms						
Protein	3644	3635	3516	3499	6908	6870
Solvent	503	454	495	294	575	504
Zinc ions	6	6	4	4	8	8
Inhibitor	34	34	17	34	68	68
B-factors						
Protein	17.7	21.6	18.8	32.0	40.4	40.6
Solvent	33.3	37.4	29.8	40.4	46.6	45.8
Zinc ions	13.0	17.4	17.2	27.9	30.3	31.6
Inhibitor	22.6	32.0	22.7	39.8	58.1	51.1
R.m.s. deviations						
Bond lengths (Å)	0.013	0.009	0.008	0.009	0.008	0.012
Bond angles (°)	1.248	0.986	1.007	0.988	0.852	1.321
Ramachandran (%)						
Outliers	0.44	0.22	0.00	0.00	0.00	0.23
Favoured	98.45	98.67	99.14	98.92	97.47	97.01

\*Values in parentheses are for highest-resolution shell.

**Table S2. Inhibitor RSCCs calculated by the PDB**

Chain	<b>L-anti-1b</b>			<b>D-syn-1b</b>		
	NDM-1	VIM-2	IMP-1	NDM-1	VIM-2	IMP-1
A	0.97	0.95	0.96	0.96	0.97	0.95
B	-	0.97	0.91	0.91	0.96	0.94
C	-	-	0.97	-	-	0.93
D	-	-	0.95	-	-	0.97

**Table S3. Interaction distances (Å) of thiazolidine inhibitors in B1 MBLs.**

Interaction	L-anti-1b			D-syn-1b		
	NDM-1	VIM-2	IMP-1	NDM-1	VIM-2	IMP-1
Zn---Zn	3.69	3.69	3.57	3.73	3.79	3.63
Thiol-Zn1	2.33	2.27	2.35	2.24	2.29	2.33
thiol-Zn2	2.35	2.26	2.34	2.32	2.25	2.2
carboxylate-Asn233 (sidechain N)	3.46	-	3.28	-	-	-
carboxylate-Asn233 (backbone N)	-	-	-	2.97	3.07	2.56
carboxylate-Arg228 (sidechain)	-	-	-	-	3.39	-
Average S-Aromatic ring at position 87*	4.81	4.17	5.51	5.11	4.33	6.58

\*Distance from the sulphur atom to the centre of the ring.

## Figures

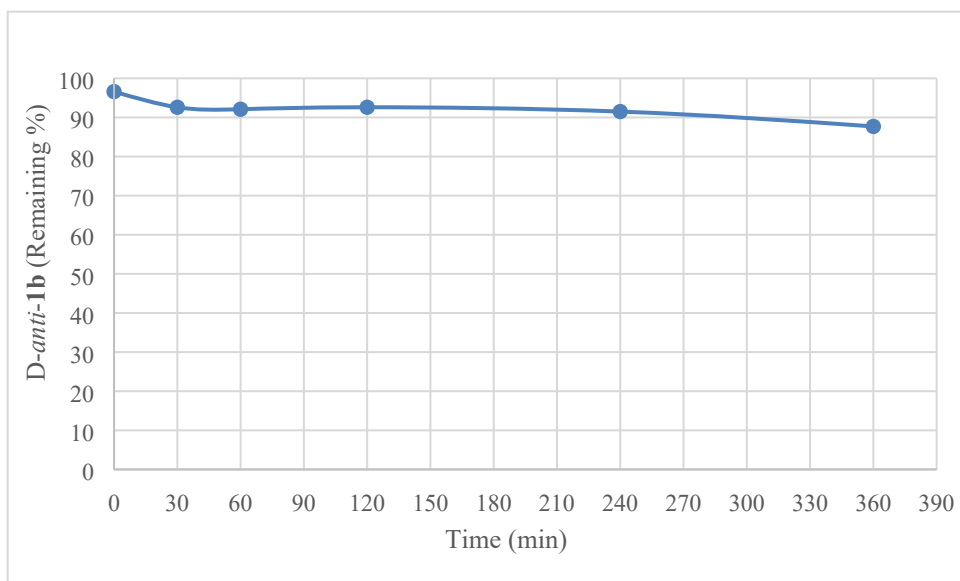


**Figure S1. Remaining D-anti-1b vs time in PBS pH 7.2 at 27°C.** Values represent the mean of triplicate measurements.

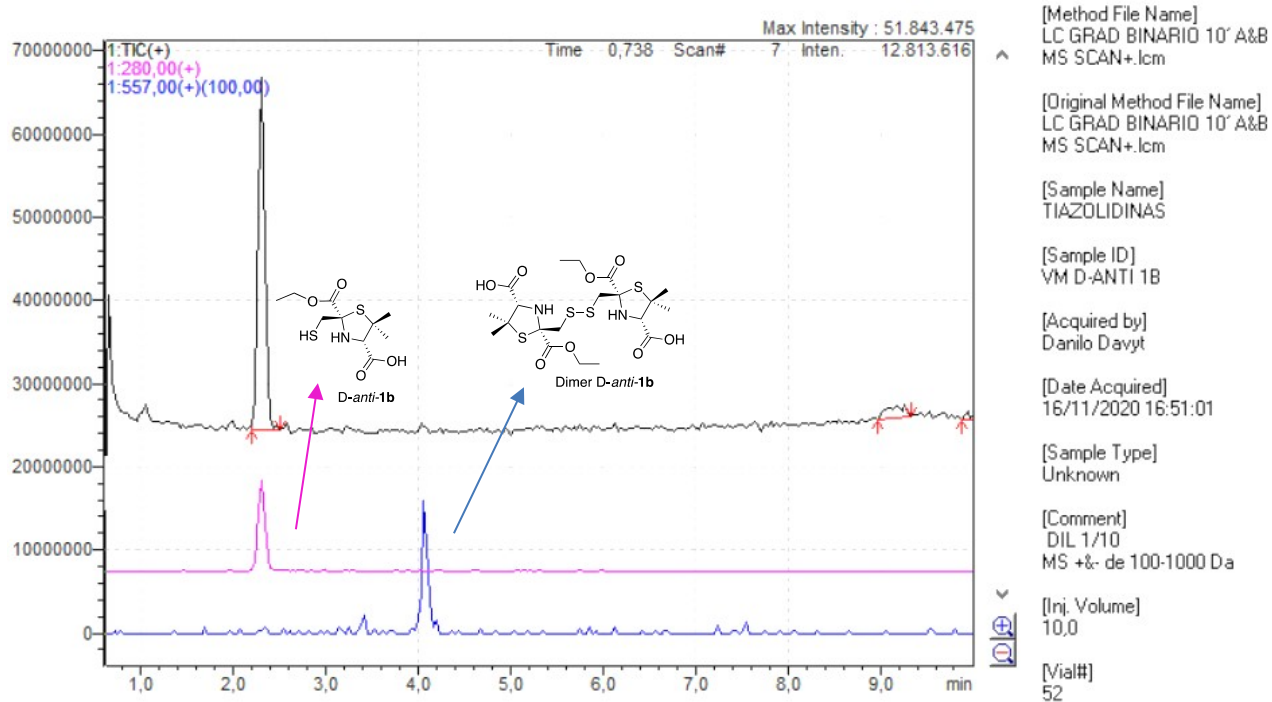


**Figure S2. Chromatogram on LCMS of D-anti-1b after 6 h incubation in PBS pH 7.2, at 27 °C.** Chromatogram in black corresponds to the Total Ion Current (TIC). Chromatogram in pink corresponds to Extracted-ion for D-anti-1b,  $[M+1]^+ = 280.0$ . Chromatogram in blue corresponds to Extracted-ion for Dimer of D-anti-1b,  $[M+1]^+ = 557.0$ .

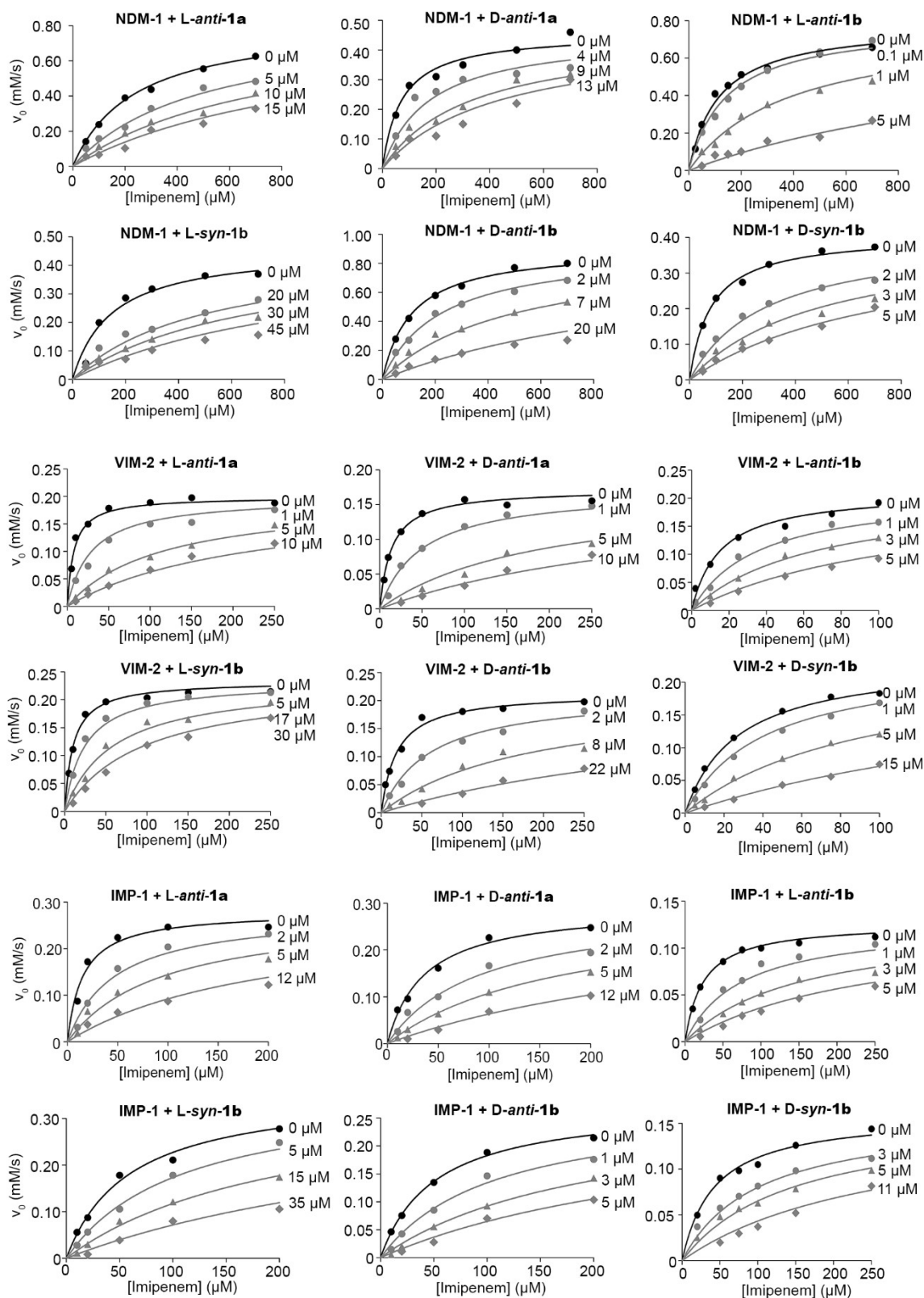


**Figure S3. Determination of the inhibition constant of MMTZ against the MBLs: NDM-1, VIM-2, and IMP-1.** Initial rates of imipenem hydrolysis were followed, in the absence and presence of the thiazolidine inhibitors. The lines show the fits to the competitive inhibition model, according to the inhibition constant ( $K_i$ ) presented in Table 2

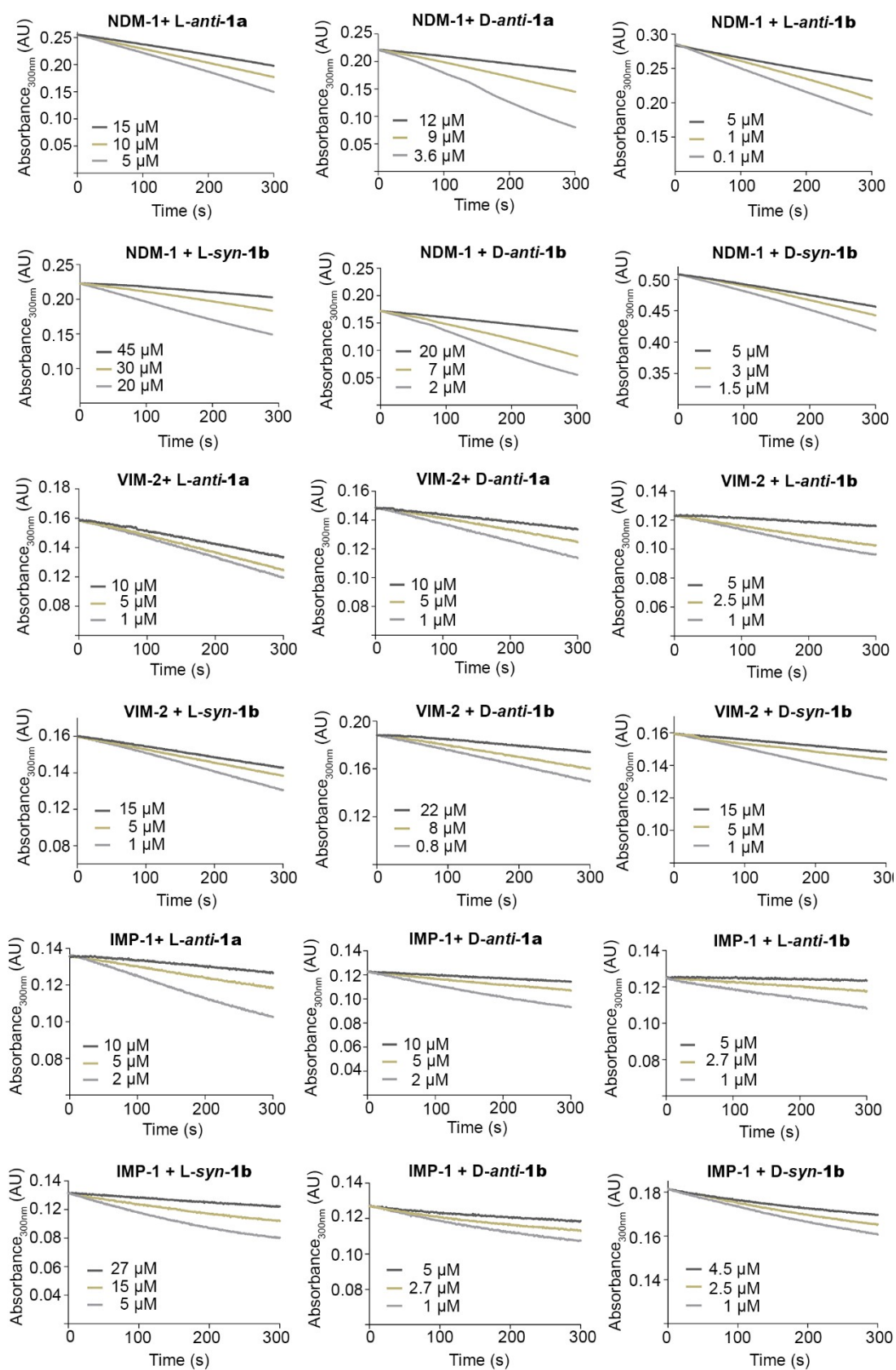


**Figure S4. Reaction curves of imipenem hydrolysis by NDM-1, VIM-2 and IMP-1 at different concentrations of the MMTZ inhibitors.**

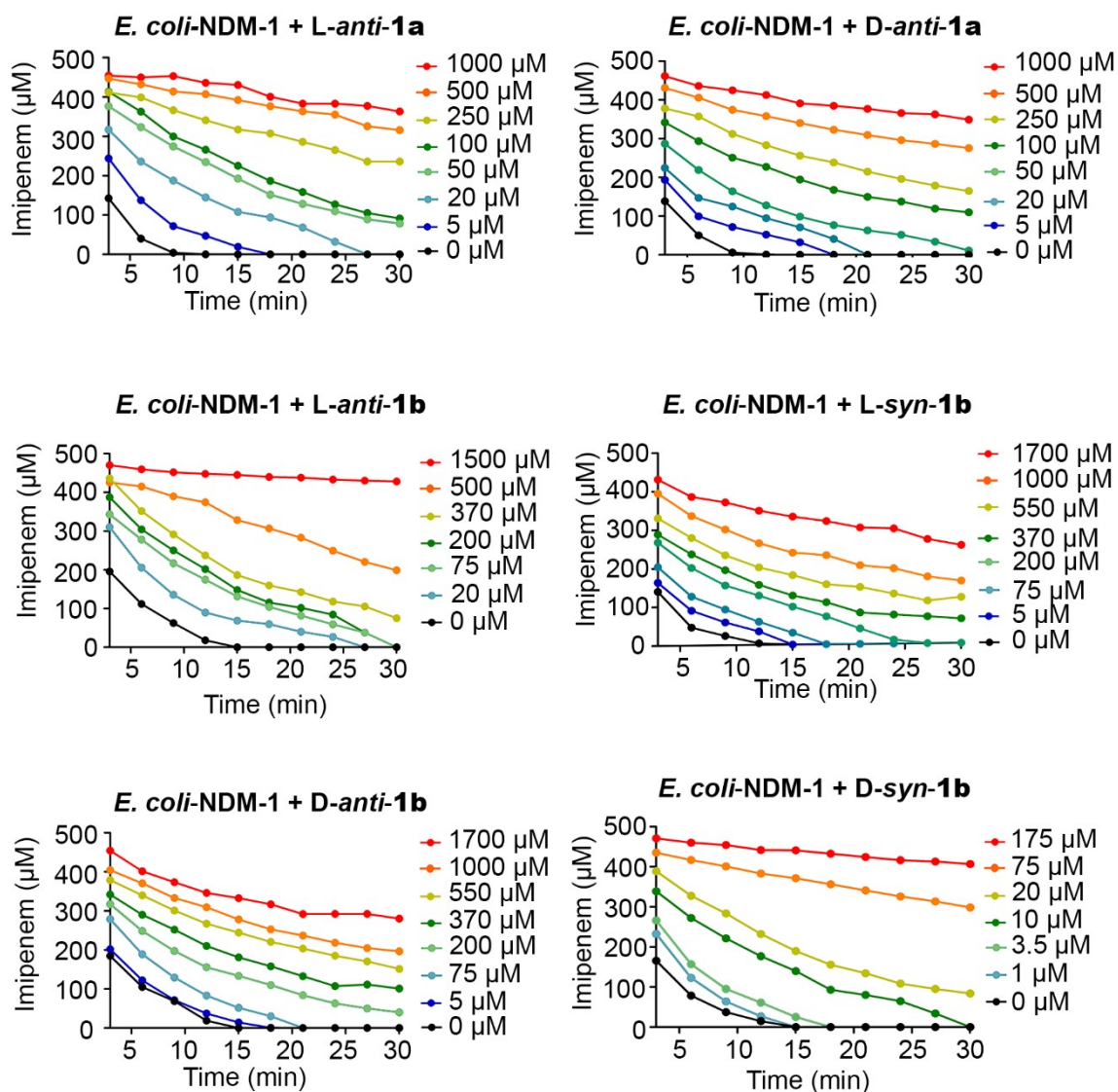


**Figure S5. Imipenem hydrolysis by *E. coli*-NDM-1.** 500  $\mu\text{M}$  Imipenem hydrolysis, by *E. coli* expressing NDM-1 ( $\text{OD}_{600}$  0.15), in the presence or absence of MMTZs inhibitors.

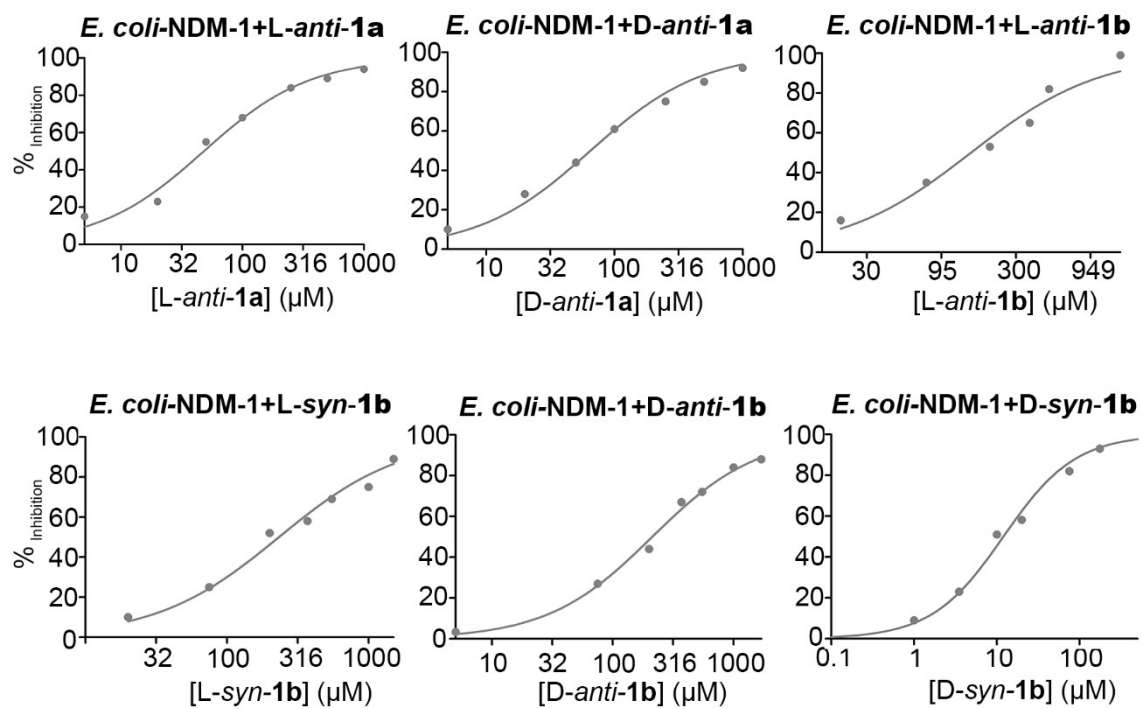


**Figure S6. In-cell IC<sub>50</sub>.** Imipenem hydrolysis by *E. coli* expressing NDM-1 (OD<sub>600</sub> 0.15) was followed in the presence or in the absence of different concentration of the MMTZs inhibitors.

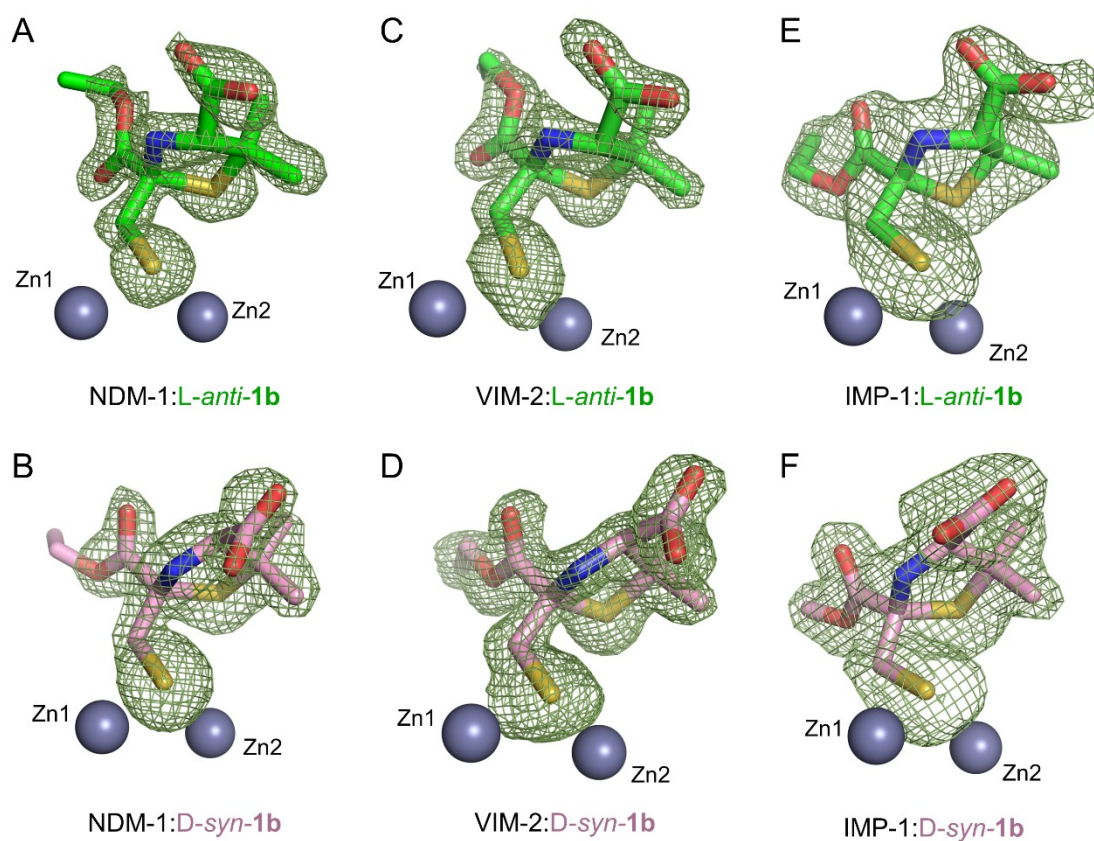


**Figure S7. Omit electron density maps of MMTZs bound in the active site of B1 MBLs.** Electron density shown is  $F_o - F_c$  (green mesh, contoured at  $3\sigma$ ) calculated after removal of inhibitor.

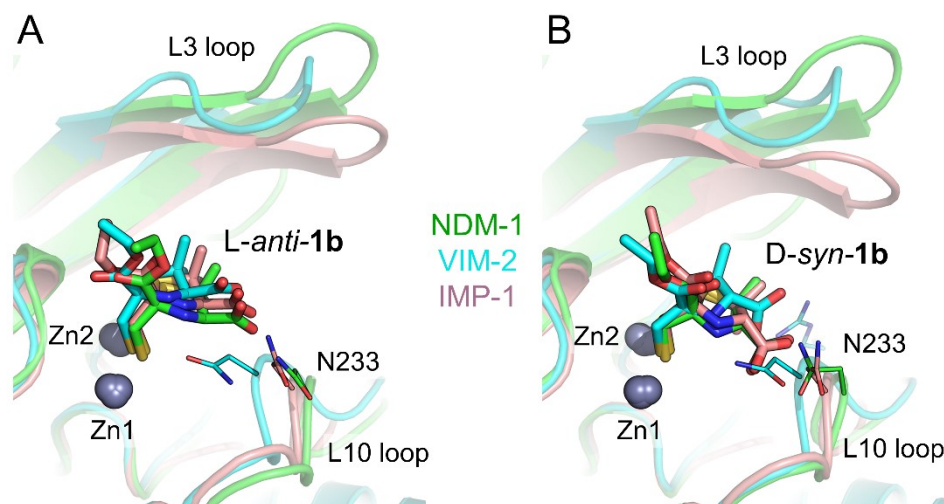


**Figure S8. Comparisons of MMTZ binding modes to B1 MBLs.** Overlays of L-*anti-1b* (A) and D-*syn-1b* (B) binding to NDM-1 (green), VIM-2 (cyan) and IMP-1 (brown). Residues making direct interactions with inhibitor (Asn233 of NDM-1/IMP-1; Arg228 of VIM-2) are shown as sticks.

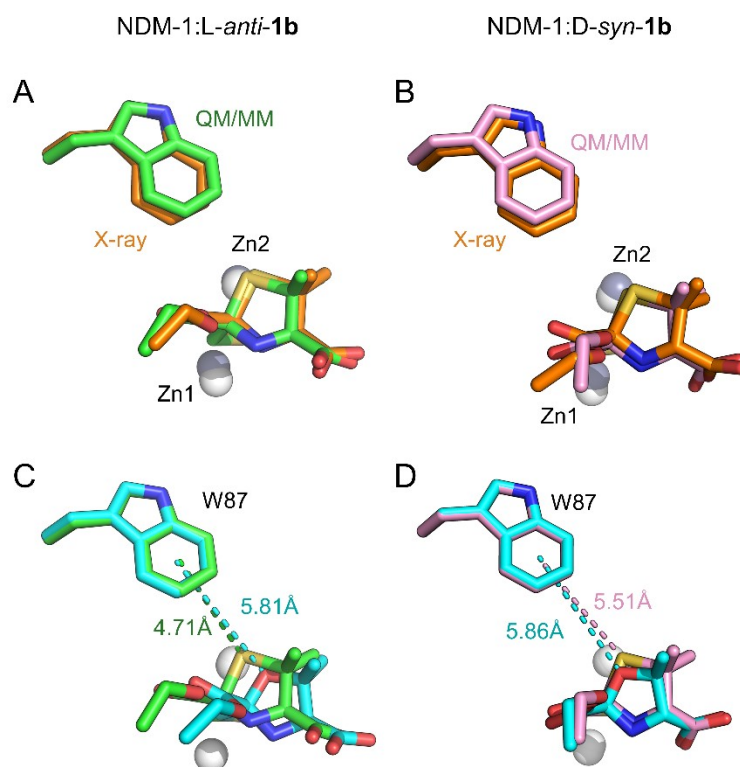


**Figure S9. Comparisons of MMTZ and MMOZ binding modes to NDM-1.** Views from the active sites of NDM-1 complexed with L-*anti*-**1b** (left) or D-*syn*-**1b** (right). **(A)** and **(B)** Overlays of QM/MM geometry optimized L-*anti*-**1a** (green) or D-*syn*-**1b** (pink) with their respective X-ray structures (PDB 6zyp and 6zyq, respectively, orange). **(C)** and **(D)** Overlays of QM/MM geometry optimized MMTZs (coloured as A and B) with their analogous QM/MM optimized MMOZs (cyan).

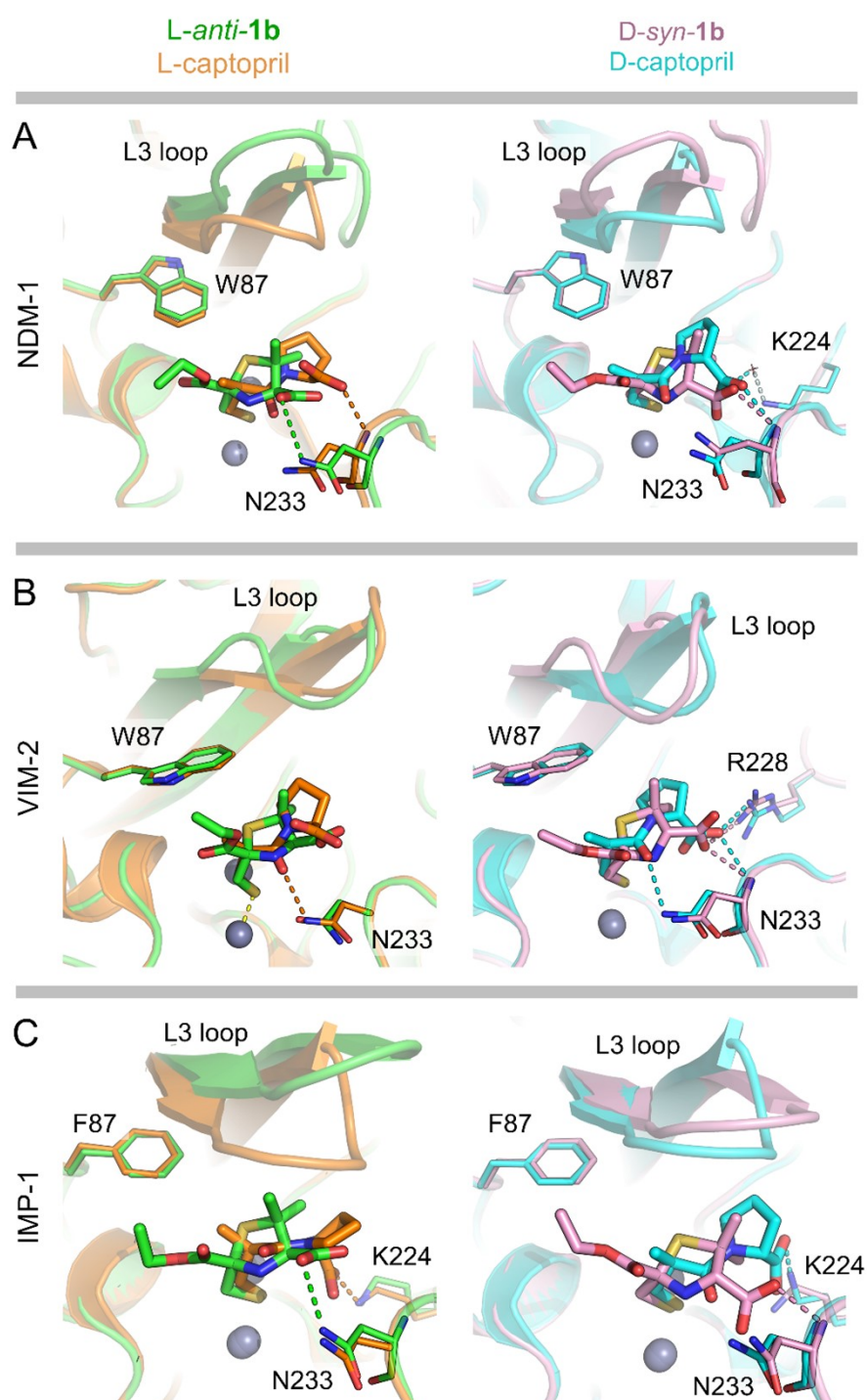


**Figure S10. Comparisons of L- and D- stereoisomers of MMTZ and captopril bound in the active sites of B1 MBLs.** Views from the active sites of B1 MBLs showing overlays on the left of L-*anti-1b* (green) with L-captopril (orange) and on the right of D-*syn-1b* (pink) with D-captopril (cyan). **(A)** NDM-1 (PDB IDs 5zio and 5zj2 for L- and D-captopril complexes, respectively); **(B)** VIM-2 (PDB IDs 4c1d<sup>1</sup> and 4c1e<sup>1</sup> for L- and D-captopril complexes, respectively); and **(C)** IMP-1 (PDB IDs 4c1f<sup>1</sup> and 4c1g<sup>1</sup> for L- and D-captopril complexes, respectively). Interactions between the inhibitor and residues in the active site are shown as dashes, coloured corresponding to the respective structure. In NDM-1, D-captopril interacts with Lys224 via a water molecule (red cross). The hydrophobic residue at position 87 (sticks, labelled) interacts with the sulphur of the thiazolidine ring of

MMTZs. Note, the five-membered thiazolidine ring of MMTZs is more deeply buried in the active site compared to captopril.

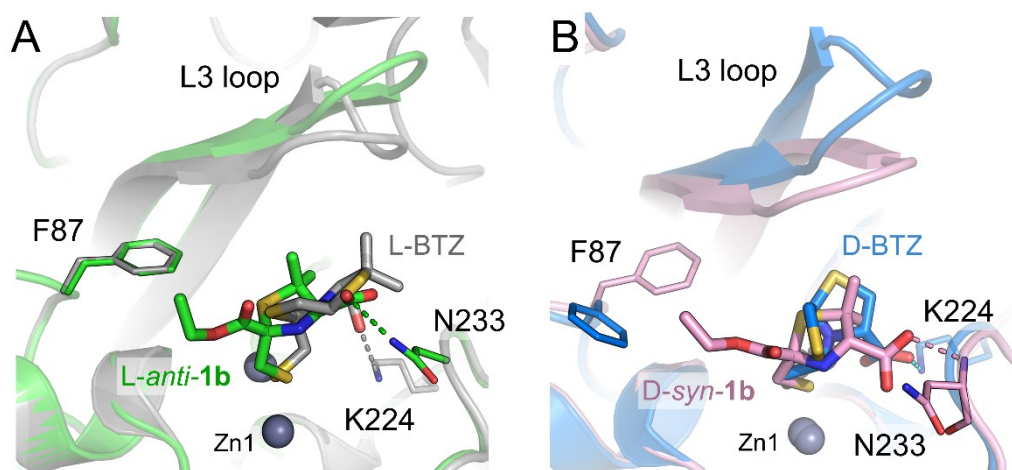


**Figure S11. MMTZ and BTZ binding to IMP-1.** Views from the active sites of IMP-1 comparing the binding modes of (A) *L-anti-1b* (green) and *L-BTZ* (grey, PDB ID 5ewa<sup>2</sup>), (B) *D-syn-1b* (pink) and *D-BTZ* (blue, PDB ID 5ev8<sup>2</sup>). Note the absence of the S-aromatic interaction for D-BTZs but conservation in the L-enantiomeric forms of MMTZs and BTZs, and D-MMTZ.

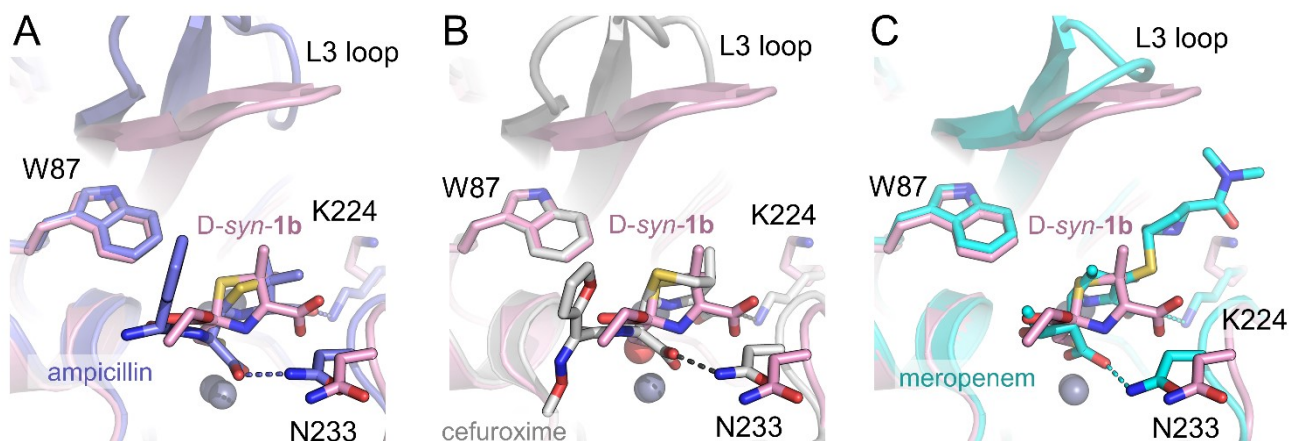


**Figure S12. Comparisons of the binding modes of MMTZ and hydrolysed antibiotic products in NDM-1.** Views from NDM-1 active sites showing overlays of *D-syn-1b* (pink) binding with the hydrolysed products of (A) ampicillin (slate, PDB ID 5zgr<sup>3</sup>), (B) cefuroxime (grey, PDB ID 5o2e<sup>4</sup>) and (C) meropenem (cyan, PDB ID 5ypm<sup>5</sup>). Interactions between hydrolysed antibiotic and NDM-1 residues Lys224 and Asn233 are shown as dashes, coloured according to structure. Note the thiazolidine, dihydrothiazine and pyrroline rings of the hydrolysed antibiotics are perpendicular to the thiazolidine ring of MMTZs.

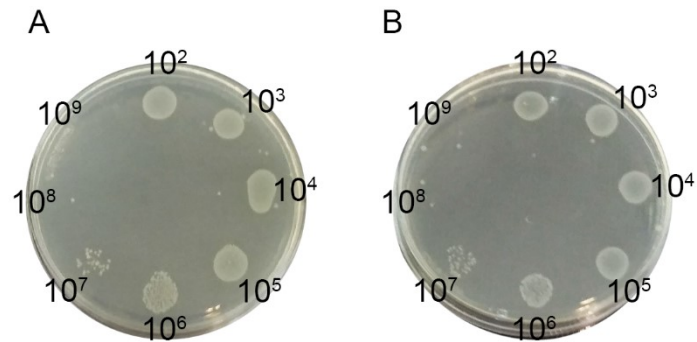


**Figure S13. Cell viability of *E. coli* expressing NDM-1 before and after the NMR experiments.** All *E. coli* cells were from the same batch. The fold of dilution of the sample prior to plating is indicated on the figure. Conditions: **(A)** cell not exposed to the treatment with 500  $\mu$ M imipenem and **(B)** cells incubated with 500  $\mu$ M imipenem after 30 min on the NMR magnet. The section labelled with  $10^7$ -fold dilution was used to evaluate cell viability, in which the same amount of single colonies was on each plate. These data demonstrated that cells were alive (viable) during the NMR experiments and that differences of cell viability are not observed.

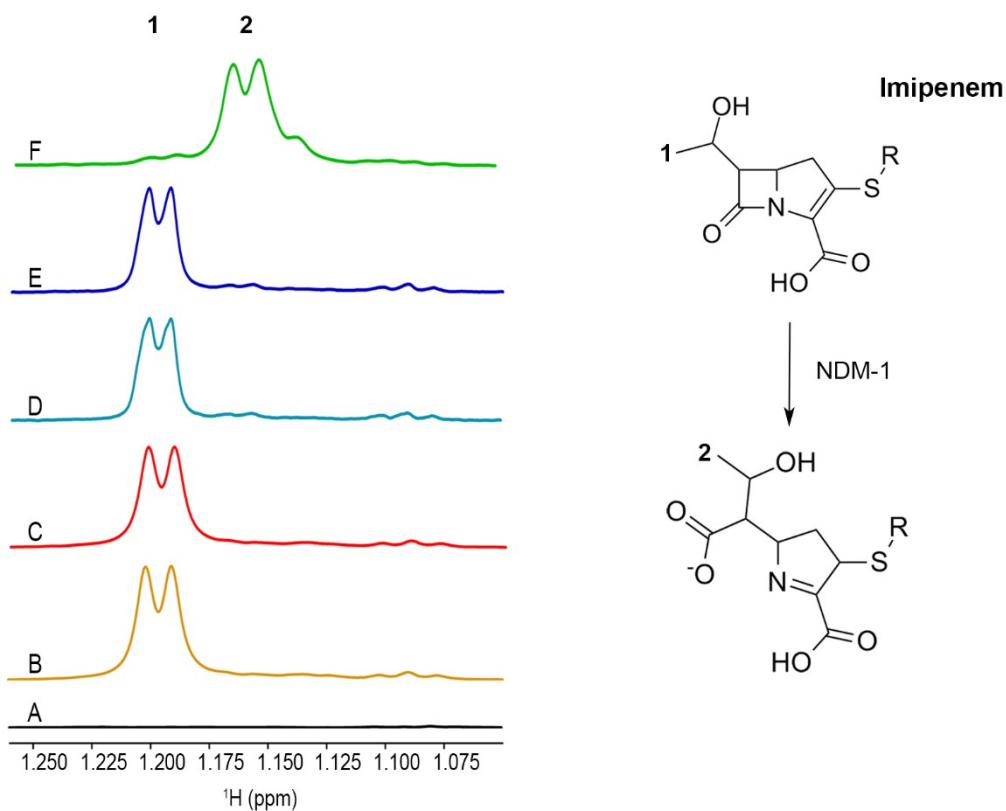
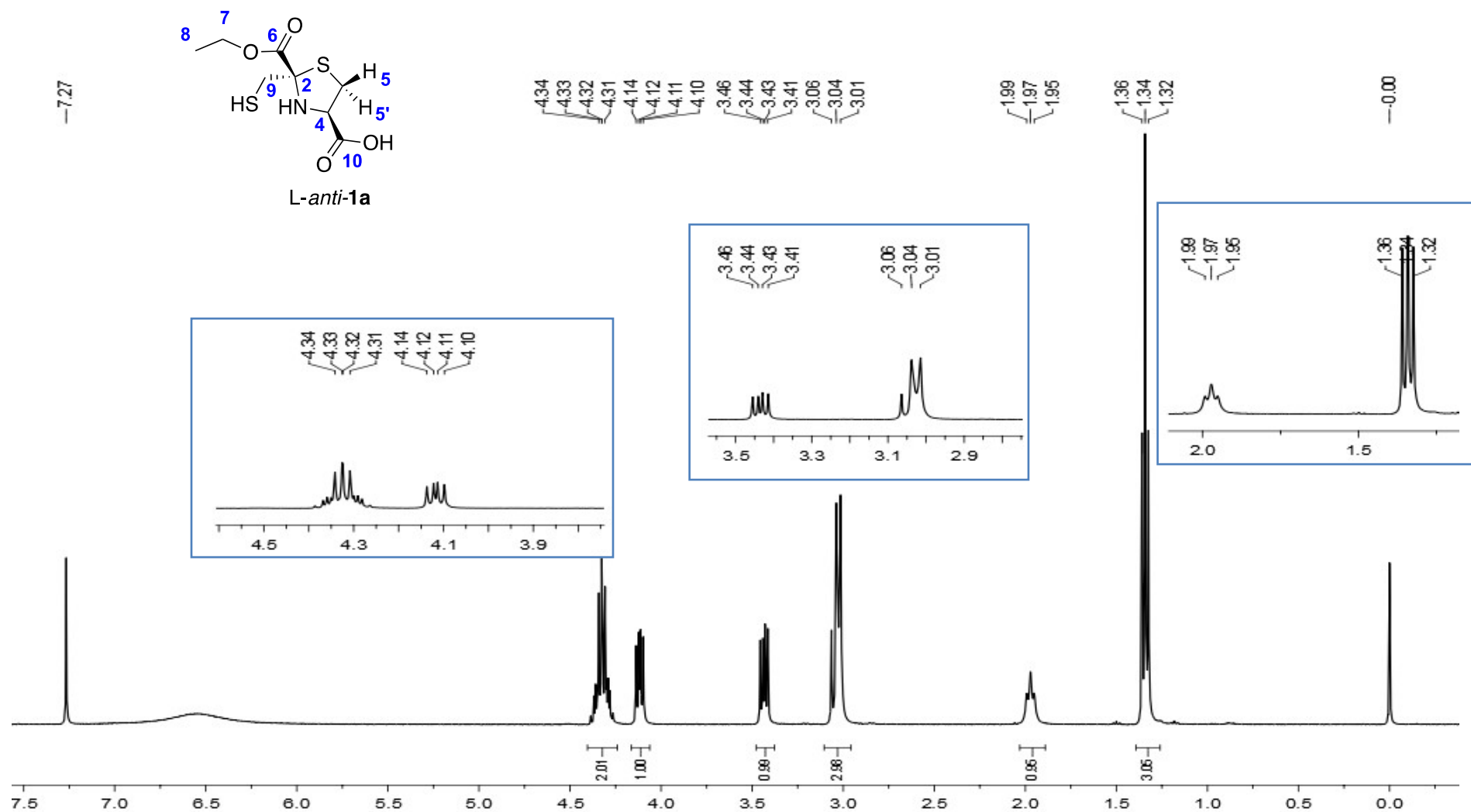
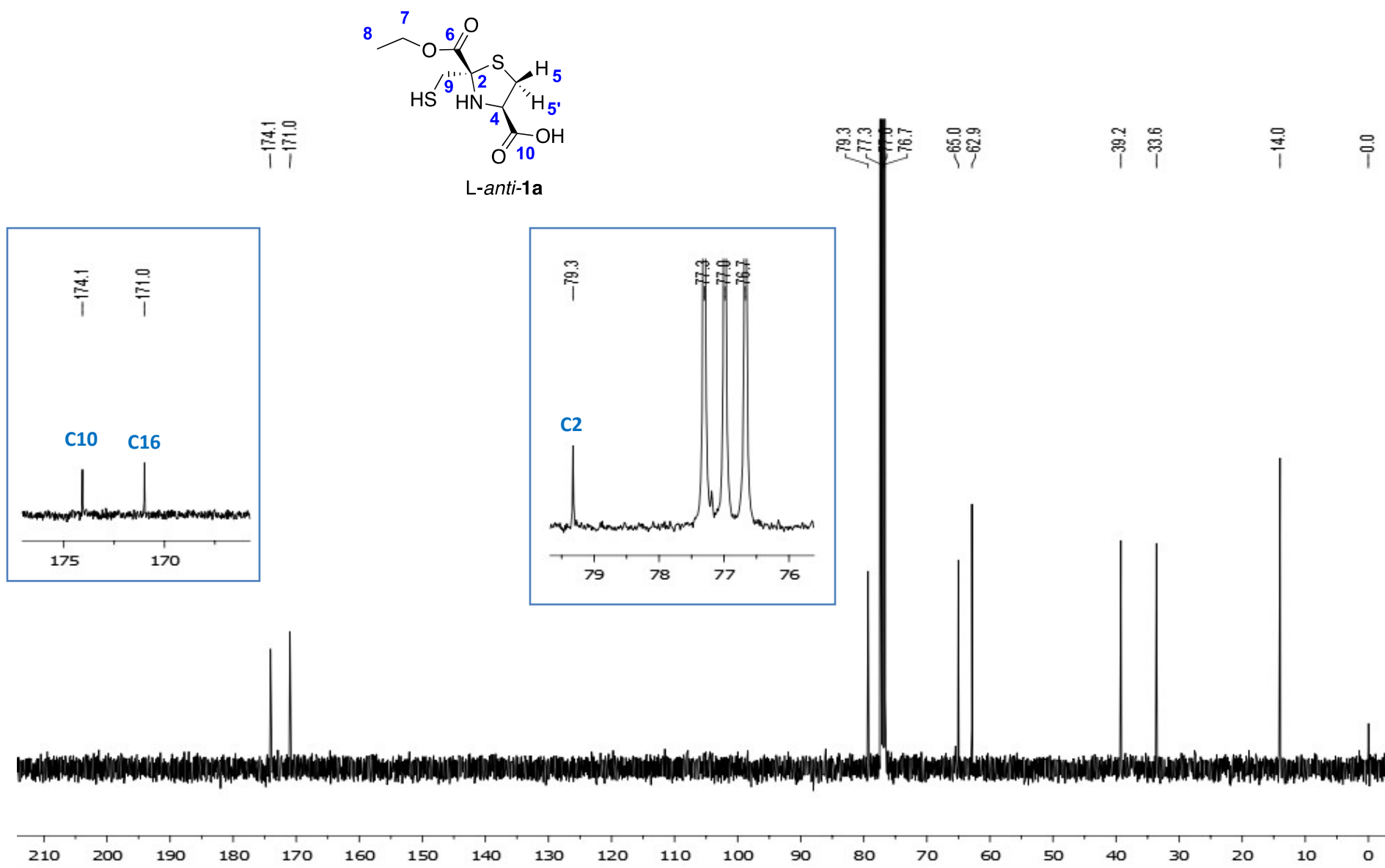


**Figure S14. Imipenem stability and hydrolysis.** (A) <sup>1</sup>H NMR spectra at 600 MHz of *E. coli* OD<sub>600</sub> 0.15, 500 μM imipenem and *E. coli*-pMBLe OD<sub>600</sub> 0.15 at (B) 0 and (C) 30 min, respectively; 500 μM imipenem and the supernatant of *E. coli* expressing NDM-1 at (D) 0 and (E) 30 min incubation time, respectively; (F) 500 μM imipenem and *E. coli* expressing NDM-1 after 30 min incubation. In order to quantify the concentration of substrate consumed or product released, we followed the signal of terminal methyl group (R1 chain) of imipenem, that when the antibiotic is hydrolysed change its position from 1.22-1.18 (substrate) to 1.17-1.12 (product).

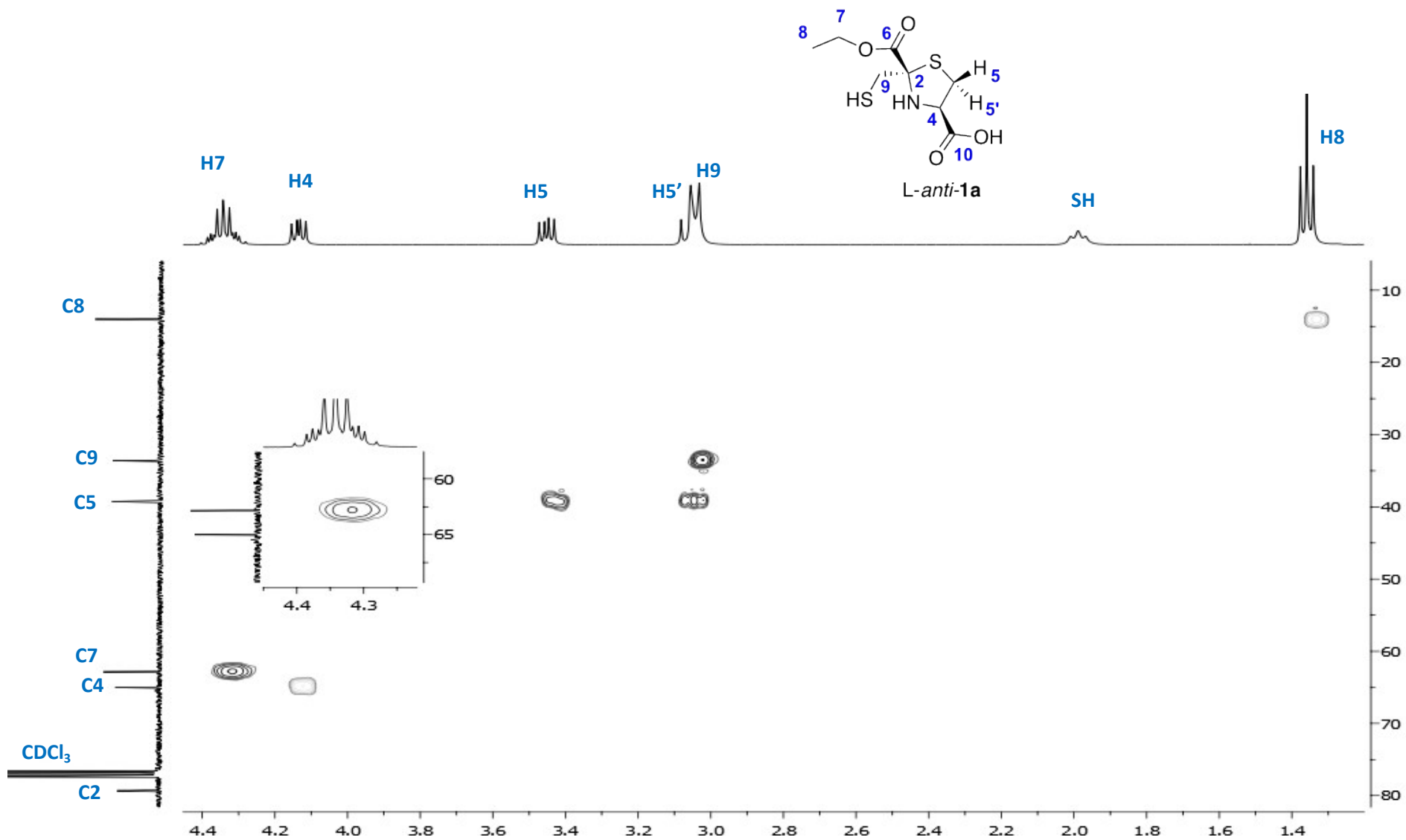
<sup>1</sup>H, <sup>13</sup>C NMR Spectra of the MMTZ inhibitors



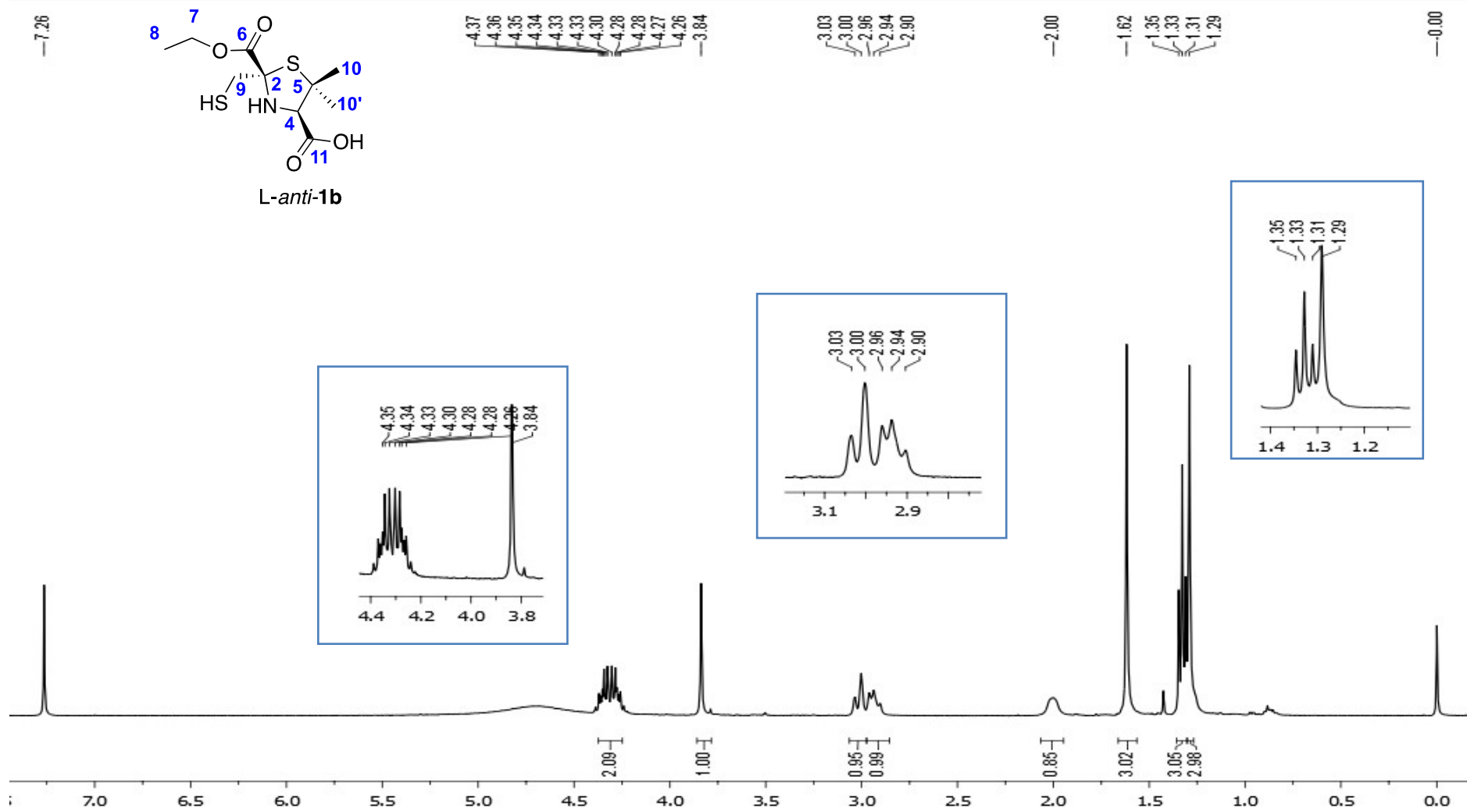
<sup>1</sup>H-NMR (400 MHz, CDCl<sub>3</sub>) spectrum of L-anti-1a



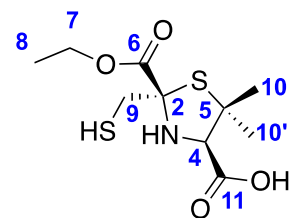
<sup>13</sup>C NMR (100 MHz, CDCl<sub>3</sub>) spectrum of L-*anti*-1a



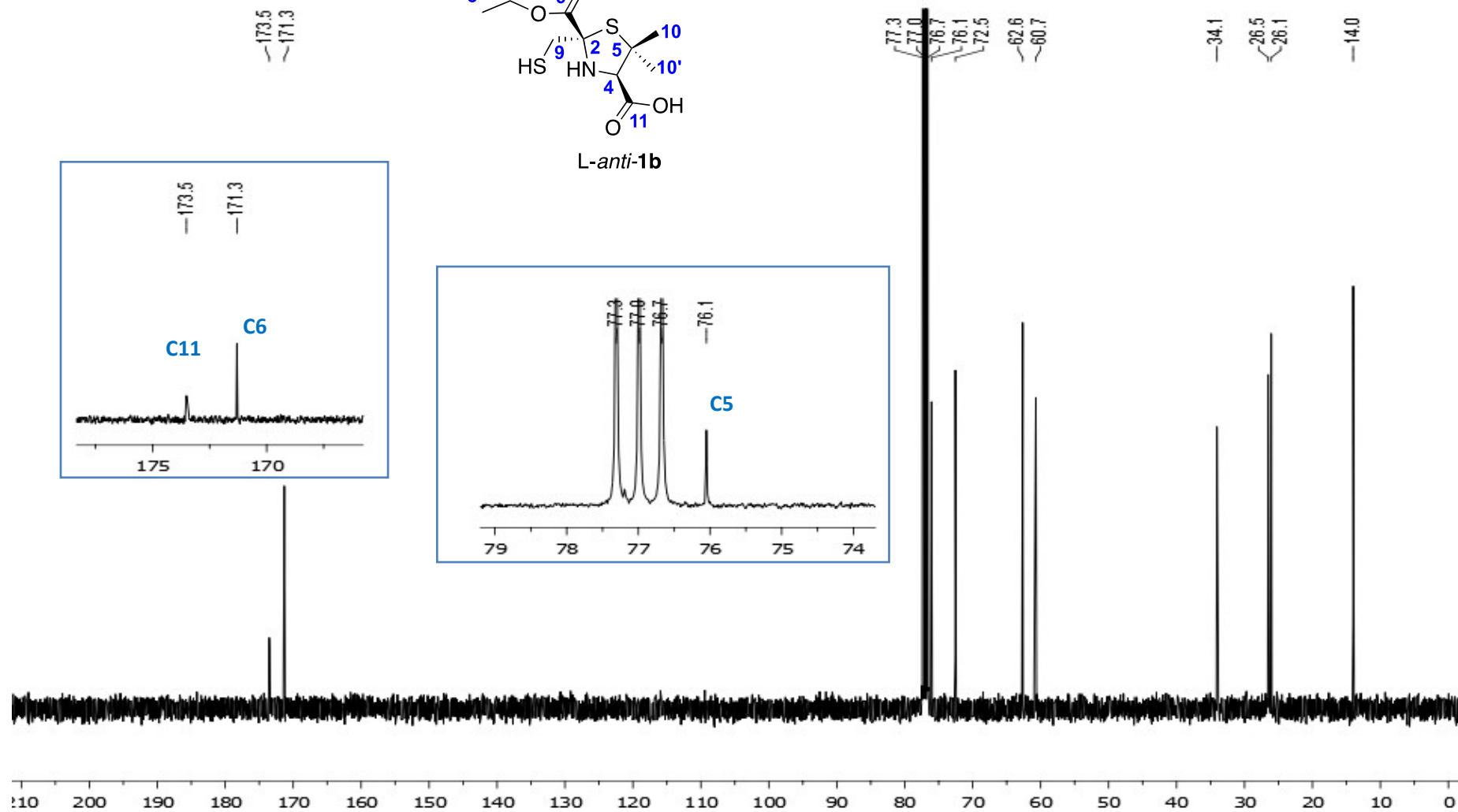
$^1\text{H}$ ,  $^{13}\text{C}$ -HSQC ( $\text{CDCl}_3$ ) spectrum of *L*-anti-**1a**, and its characterization.



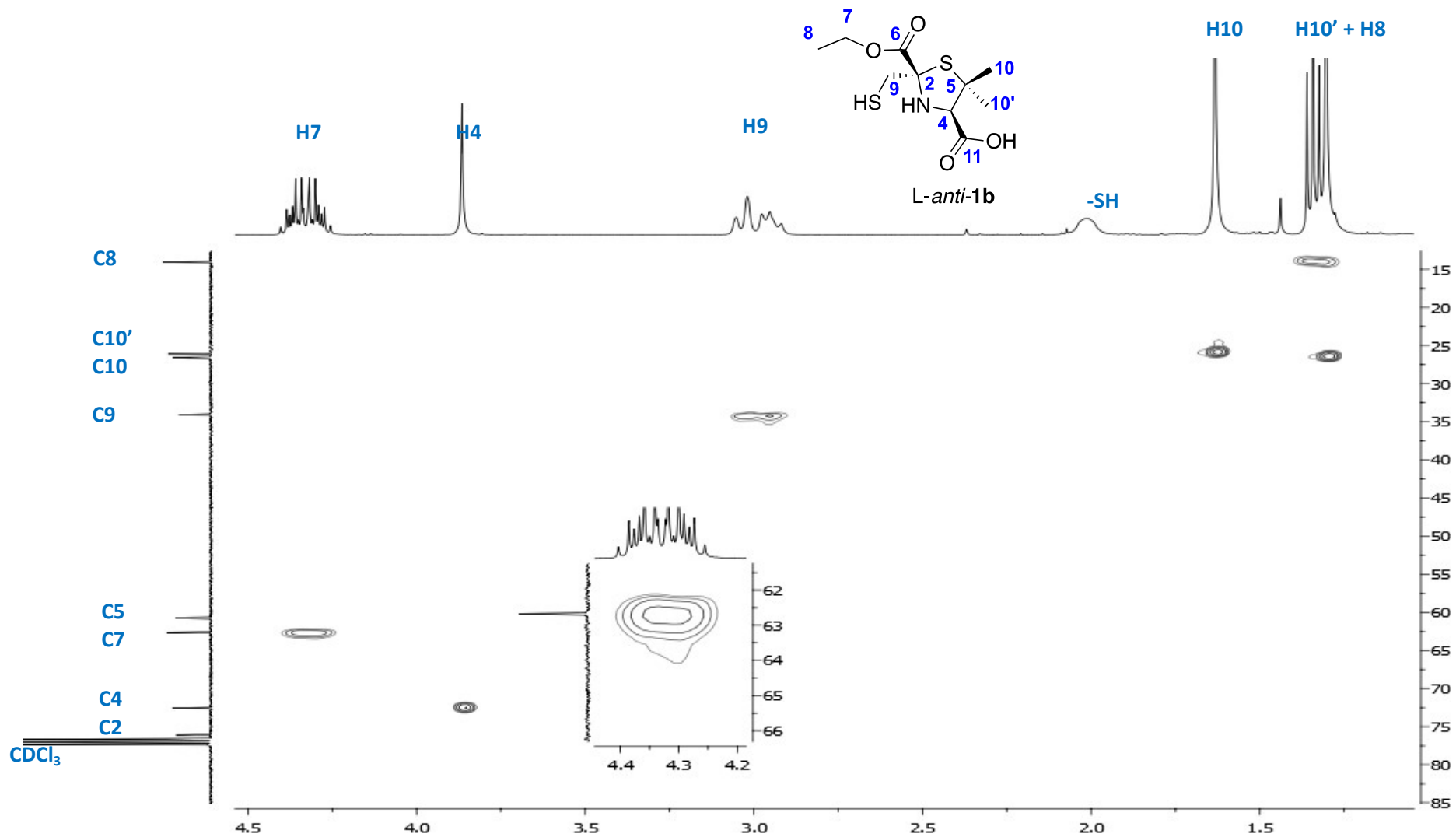
<sup>1</sup>H-NMR (400 MHz, CDCl<sub>3</sub>) spectrum of L-anti-1b



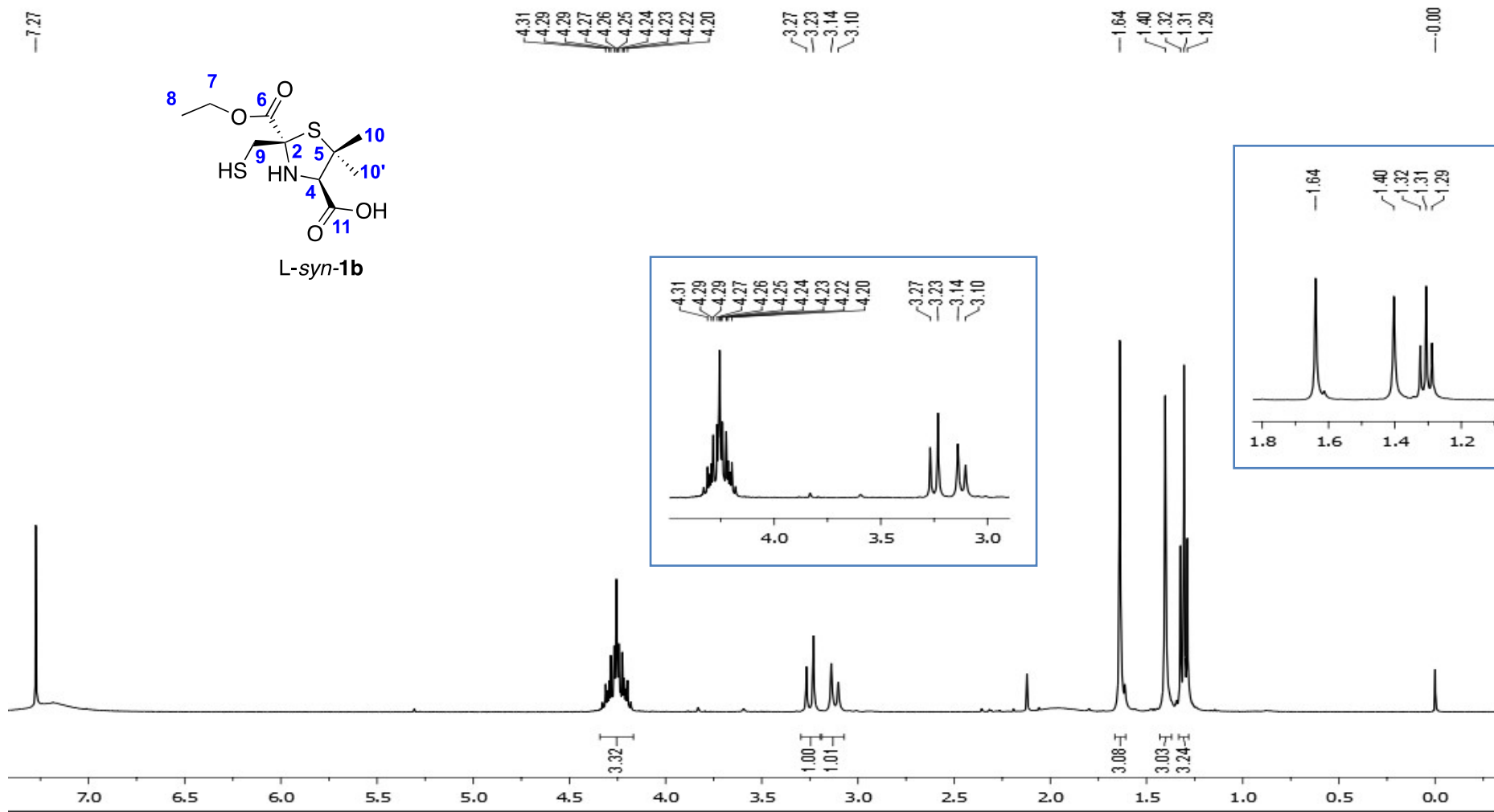
L-anti-1b



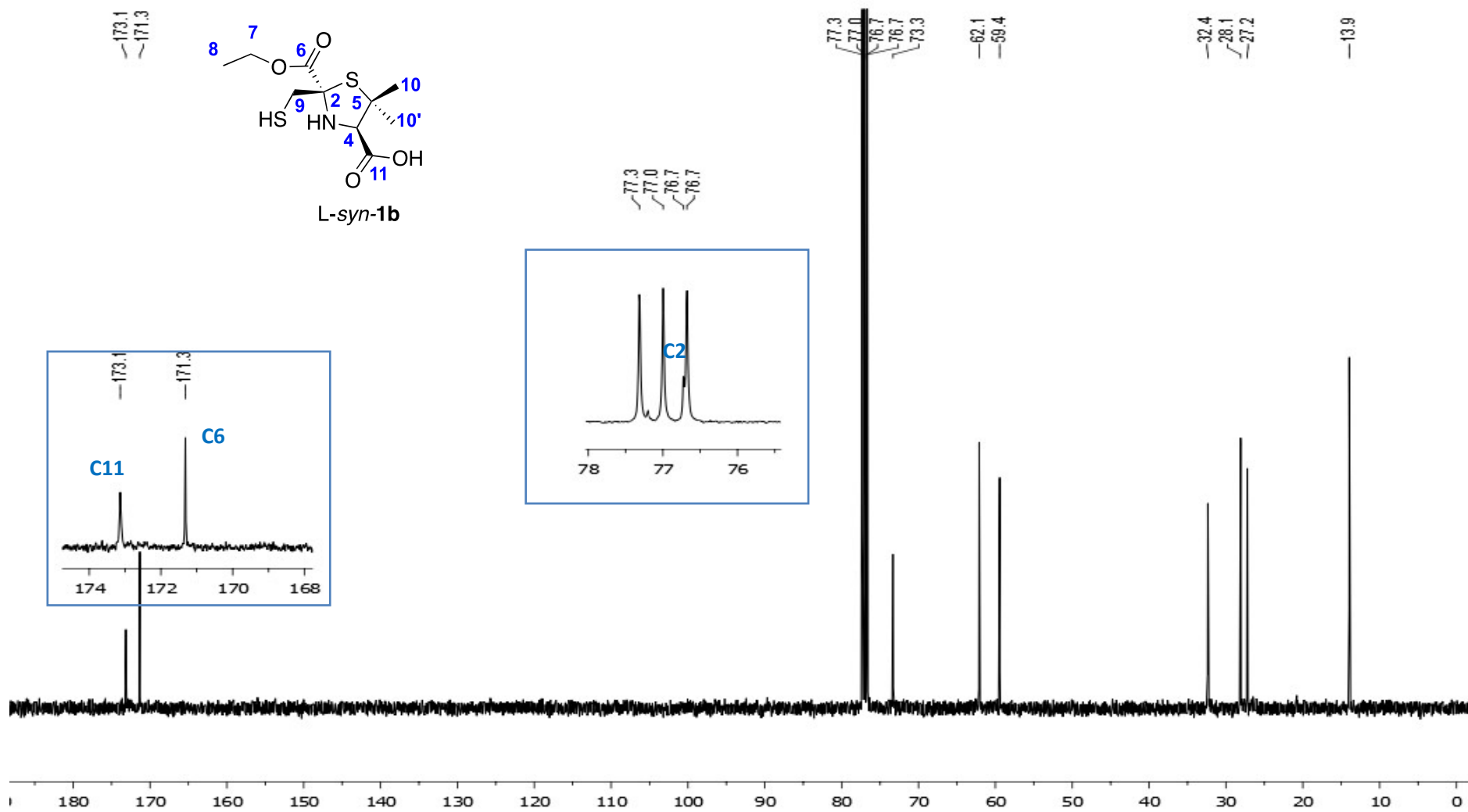
$^{13}\text{C}$  NMR (100 MHz,  $\text{CDCl}_3$ ) spectrum of L-anti-1b



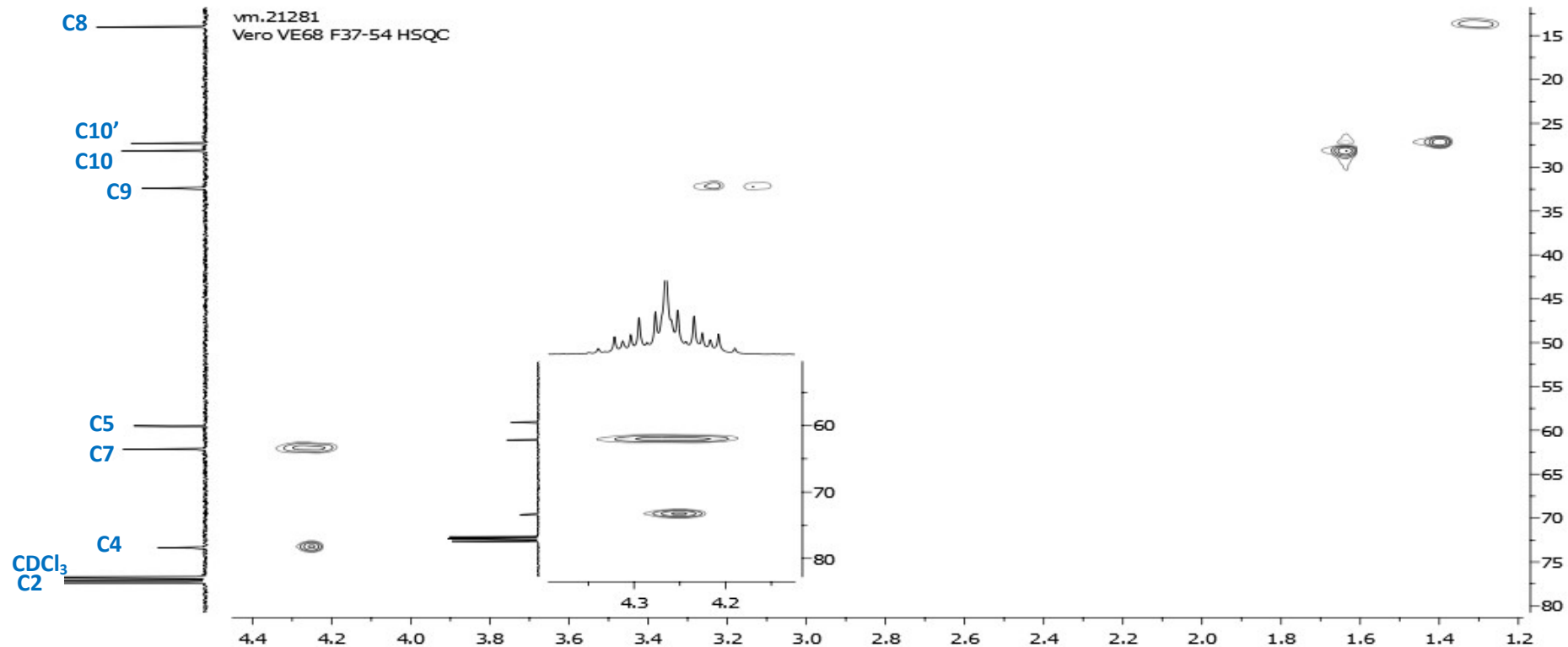
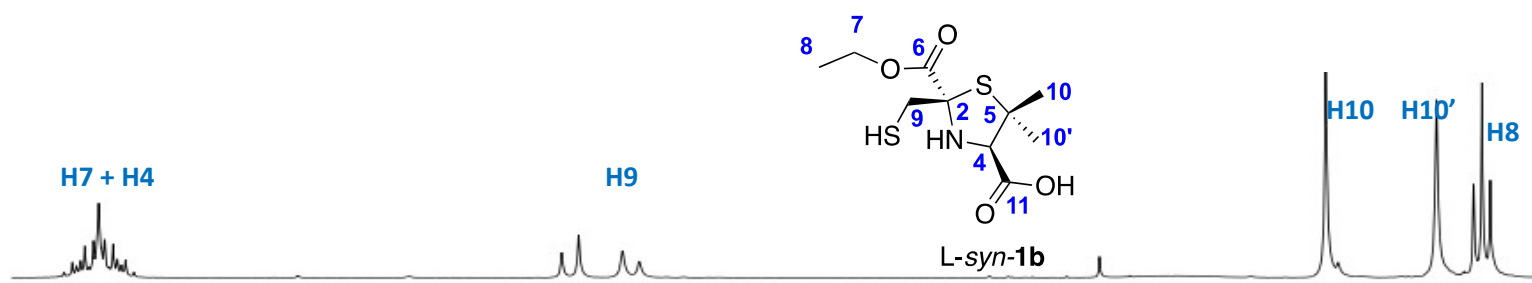
$^1\text{H}$ ,  $^{13}\text{C}$ -HSQC ( $\text{CDCl}_3$ ) spectrum of *L-anti-1b*, and its characterization.



<sup>1</sup>H-NMR (400 MHz, CDCl<sub>3</sub>) spectrum of L-syn-1b



<sup>13</sup>C NMR (100 MHz, CDCl<sub>3</sub>) spectrum of L-syn-1b



<sup>1</sup>H, <sup>13</sup>C-HSQC (CDCl<sub>3</sub>) spectrum of L-syn-1b, and its characterization.

## Crystal data and structure refinement of *L-anti-1a*

*L-anti-1a*: The crystal structure of compound Data Block Name: data\_mo\_Mario\_Valerie\_0m Unit Cell Parameters: a 6.9704(3) b 8.0097(3) c 11.9695(5) P21 has been deposited at the Cambridge Crystallographic Data Centre (CCDC 2017238).

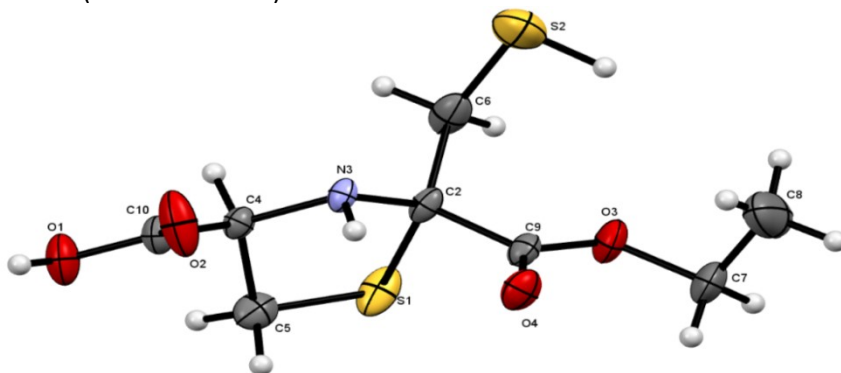


**Figure S15: ORTEP.** Molecular structure of *L-anti-1a* obtained by monocrystal X ray.

A specimen of  $C_{10}H_{13}F_2NO_4S_2$ , approximate dimensions 0.168 mm x 0.289 mm x 0.450 mm, was used for the X-ray crystallographic analysis. The X-ray intensity data was measured and a total of 679 frames were collected. The total exposure time was 16.68 hs. The frames were integrated with the Bruker SAINT software package using a narrow-frame algorithm. The integration of the data using a monoclinic unit cell yielded a total of 22754 reflections to a maximum  $\vartheta$  angle of 28.34° (0.75 Å resolution), of which 3271 were independent (average redundancy 6.956, completeness = 99.4 %,  $R_{int}$  = 2.62 %,  $R_{sig}$  = 1.82 %) and 3071 (93.89 %) were greater than  $2\sigma(F_2)$ . The final cell constants of  $a = 6.9704(3)$  Å,  $b = 8.0097(3)$  Å,  $c = 11.9695(5)$  Å,  $\beta = 100.105(2)$  ° and volume = 657.90(5) Å<sup>3</sup>, are based upon the refinement of the XYZ-centroids of 9963 reflections above with  $5.937^\circ < 2\vartheta < 56.649^\circ$ . Data were corrected for absorption effects using the multi-scan method (SADABS). The ratio of minimum to maximum apparent transmission was 0.907. The calculated minimum and maximum transmission coefficients (based on crystal size) are 0.8270 and 0.93. The final anisotropic full-matrix least-squares refinement on F<sub>2</sub> with 207 variables converged at  $R_1 = 3.24$  %, for the observed data and  $wR_2 = 8.92$  % for all data. The goodness-of-fit was 1.114. The largest peak in the final difference electron density synthesis was 0.237 e<sup>-</sup>/Å<sup>3</sup> and the largest hole was -0.236 e<sup>-</sup>/Å<sup>3</sup> with an RMS deviation of 0.052 e<sup>-</sup>/Å<sup>3</sup>. On the basis of the final model, the calculated density was 1.582 g/cm<sup>3</sup> and  $F(000)$ , 324 e<sup>-</sup>.

**Table S4. Sample and crystal data.**

Compound	L- <i>anti</i> -1a	
Identification code	Mario_Valerie	
Chemical formula	C <sub>10</sub> H <sub>13</sub> F <sub>2</sub> NO <sub>4</sub> S <sub>2</sub>	
Formula weight	313.33 g/mol	
Temperature	298(2) K	
Wavelength	0.71073 Å	
Crystal size	0.168 x 0.289 x 0.450 mm	
Crystal system	monoclinic	
Space group	P 1 21 1	
Unit cell dimensions	a = 6.9704(3) Å	α = 90°
	b = 8.0097(3) Å	β = 100.105(2)°
	c = 11.9695(5) Å	γ = 90°
Volume	657.90(5) Å <sup>3</sup>	
Z	2	
Density (calculated)	1.582 g/cm <sup>3</sup>	
Absorption coefficient	0.438 mm <sup>-1</sup>	
F(000)	324	

**Table S5. Data collection and structure refinement.**

Compound	L- <i>anti</i> -1a	
Theta range for data collection	2.97 to 28.34°	
Index ranges	-9<=h<=9, -10<=k<=10, -15<=l<=15	
Reflections collected	22754	
Independent reflections	3271 [R(int) = 0.0262]	
Coverage of independent reflections	99.4%	
Absorption correction	multi-scan	
Max. and min. transmission	0.9300 and 0.8270	
Refinement method	Full-matrix least-squares on F <sup>2</sup>	
Refinement program	SHELXL-2014/6 (Sheldrick, 2014)	
Function minimized	Σ w(F <sub>o</sub> <sup>2</sup> - F <sub>c</sub> <sup>2</sup> ) <sup>2</sup>	
Data / restraints / parameters	3271 / 43 / 207	
Goodness-of-fit on F <sup>2</sup>	1.114	
Δ/σ <sub>max</sub>	0.001	
Final R indices	3071 data; I>2σ(I)	R1 = 0.0324, wR2 = 0.0846
	all data	R1 = 0.0362, wR2 = 0.0892
Weighting scheme	w=1/[σ <sup>2</sup> (F <sub>o</sub> <sup>2</sup> )+(0.0426P) <sup>2</sup> +0.2284P] where P=(F <sub>o</sub> <sup>2</sup> +2F <sub>c</sub> <sup>2</sup> )/3	
Absolute structure parameter	-0.0(0)	
Largest diff. peak and hole	0.237 and -0.236 eÅ <sup>-3</sup>	
R.M.S. deviation from mean	0.052 eÅ <sup>-3</sup>	

**Table S6. Hydrogen bond distances (Å) and angles (°) for L-*anti*-1a.**

	<b>Donor-H</b>	<b>Acceptor-H</b>	<b>Donor-Acceptor</b>	<b>Angle</b>
O5-H5...O4	0.82	2.05	2.791(4)	149.5
O5-H5...N1	0.82	2.21	2.722(3)	120.

## HPLC Purity.

The purity of all compounds was determined by HPLC at 1 mg/mL concentration.

HPLC for determination of the purity of compound *L-anti-1a* and *D-anti-1b* was performed on a Shimadzu with binary pump system and variable  $\lambda$  detector, using Phenomenex Luna C18 column (4.6mm x 150 mm, 5  $\mu$ m). The solvent was MeCN (0.05 % Formic acid) as mobile phase A and H<sub>2</sub>O (0.05 % Formic acid) as mobile phase B at a flow rate of 1 mL/min. The gradient program was as follows: 50-99 %A (0-10 min), 99 %A (10-12 min) and 99-50 %A (12.01-15 min). The column temperature was maintained at 25°C, and the UV wavelength for detection was 215 nm.

HPLC for determination of the purity of compound *D-anti-1a* and *L-anti-1b* was performed on a Waters 2996, PDA detector and Binary Pump system, Phenomenex Luna C18 column (4.6 mm x 150 mm, 5  $\mu$ m). The solvent was 99 % MeCN (0.05 % Formic acid) as mobile phase A and H<sub>2</sub>O (0.05 % Formic acid) as mobile phase B at a flow rate of 1 mL/min. The column temperature was used at room temperature, and the UV wavelength for detection was 215 nm. The gradient program was as follows: 50-99 % A (0-10min), 99 % A (10-12 min) and 50 % A (12.01-15 min).

HPLC for determination of the purity of compound *L-syn-1b* and *D-syn-1b* was performed on a Shimadzu with binary pump system and variable  $\lambda$  detector, using Phenomenex Kinetex C18 column (4.6 mm x 150 mm, 5  $\mu$ m). Gradient of MeCN (0.05 % Formic acid) as mobile phase A and H<sub>2</sub>O (0.05 % Formic acid) as mobile phase B at a flow rate of 1 mL/min was used. The gradient program was as follows: 50-99 %A (0-10 min), 99 %A (10-12 min) and 99-50 %A (12.01-15 min). The column temperature was maintained at 25°C, and the UV wavelength for detection was 215 nm.

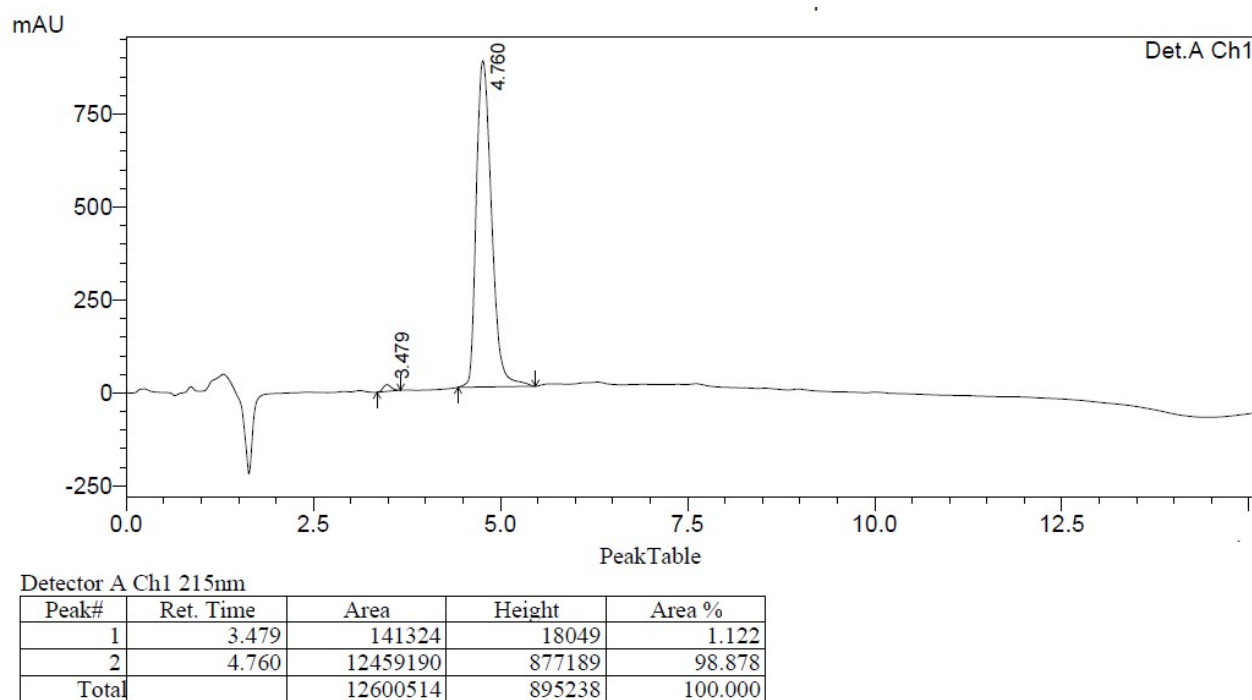
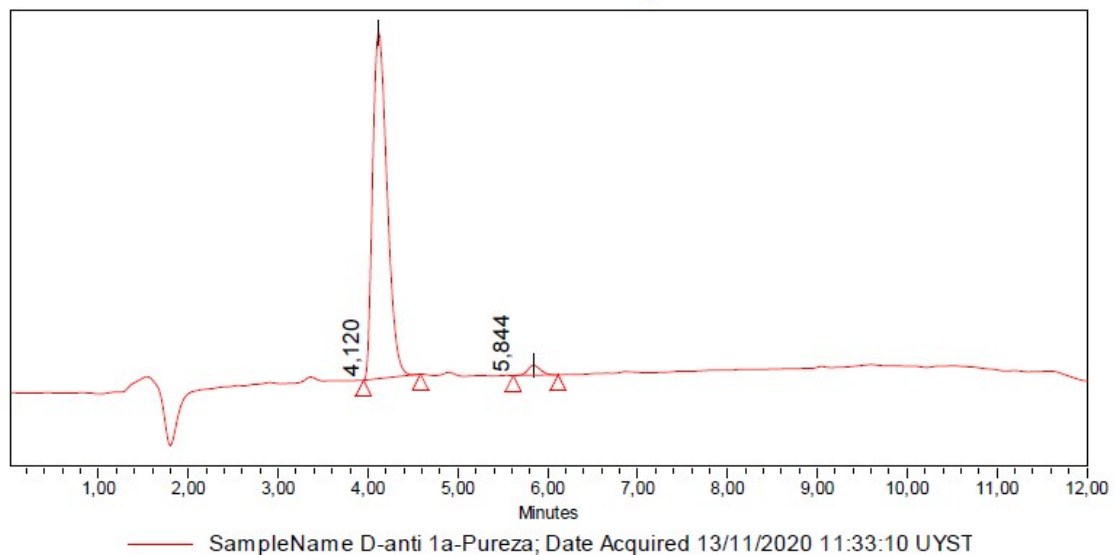


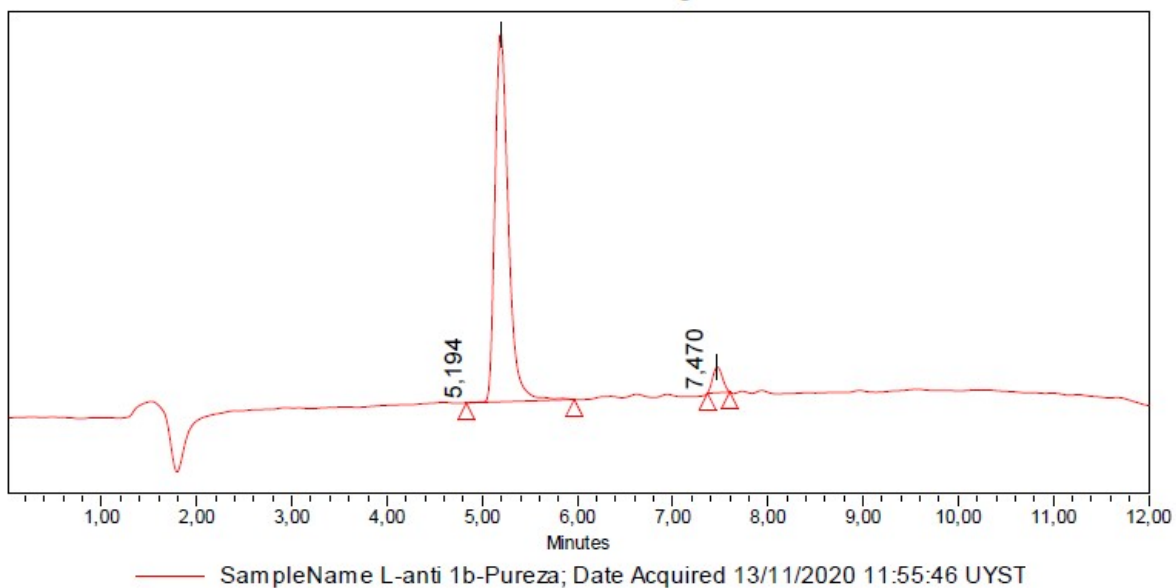
Figure S16: Chromatogram of compound *L-anti-1a*, monitored at 215 nm



**Peak Results**

	Name	RT	Area	Height	Injection	% Area
1		4,120	9905803	890416	1	97,56
2		5,844	248048	25175	1	2,44
Mean			5076925,5			
% RSD			134,5			

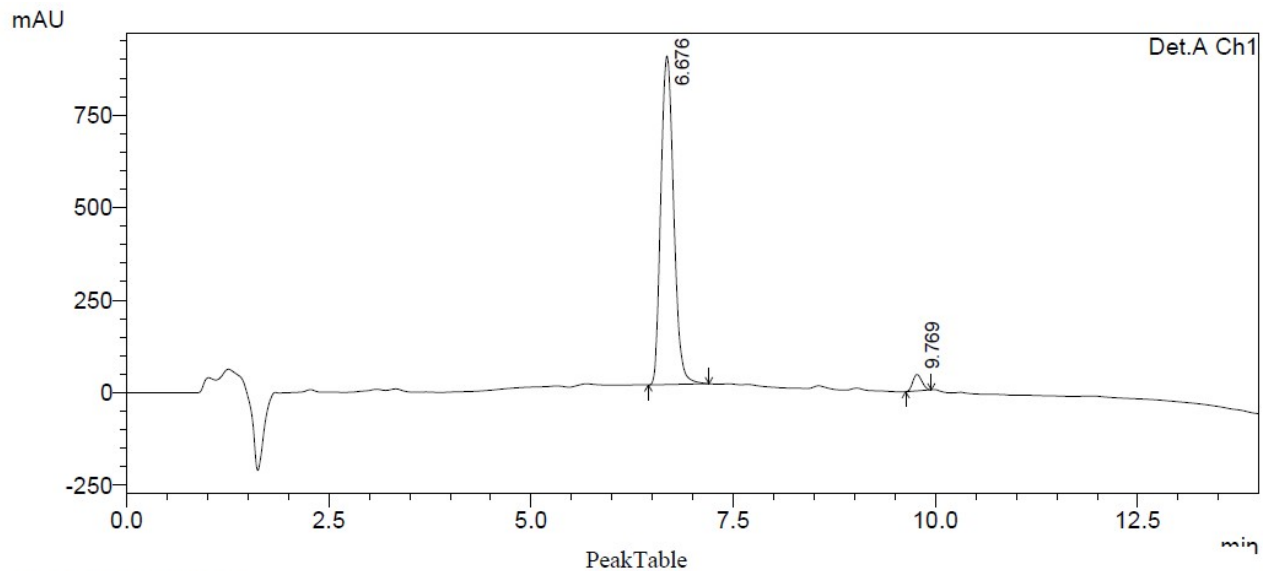
Figure S17: Chromatogram of compound D-*anti*-1a, monitored at 215 nm



**Peak Results**

	Name	RT	Area	Height	Injection	% Area
1		5,194	8671434	884250	2	95,18
2		7,470	439029	61973	2	4,82
Mean			4555231,5			
% RSD			127,8			

Figure S18: Chromatogram of compound L-*anti*-1b, monitored at 215 nm



Detector A Ch1 215nm

Peak#	Ret. Time	Area	Height	Area %
1	6.676	9818347	886936	96.568
2	9.769	348958	44006	3.432
Total		10167306	930942	100.000

Figure S19: Chromatogram of compound D-anti-1b, monitored at 215 nm

PeakTable

Detector A Ch1 215nm

Peak#	Name	Ret. Time	Area	Height	Area %	Height %
1		2.254	118473	15644	3.548	4.868
2		2.635	3220772	305727	96.452	95.132
Total			3339245	321371	100.000	100.000

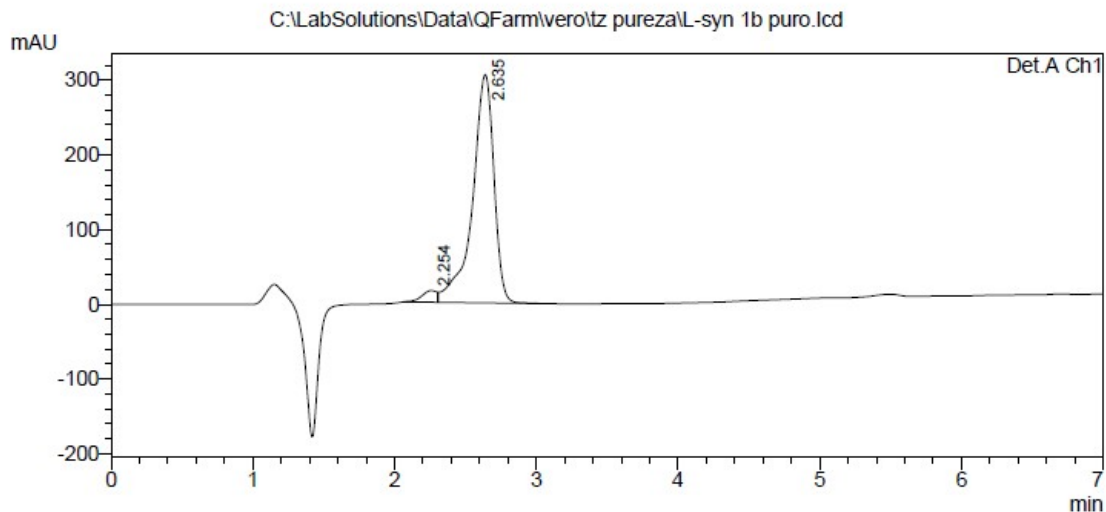


Figure S20: Chromatogram of compound L-syn-1b, monitored at 215 nm

PeakTable

Detector A Ch1 215nm

Peak#	Ret. Time	Area	Height	Area %	Height %
1	2.248	128030	13973	3.829	4.388
2	2.644	3215436	304467	96.171	95.612
Total		3343466	318441	100.000	100.000

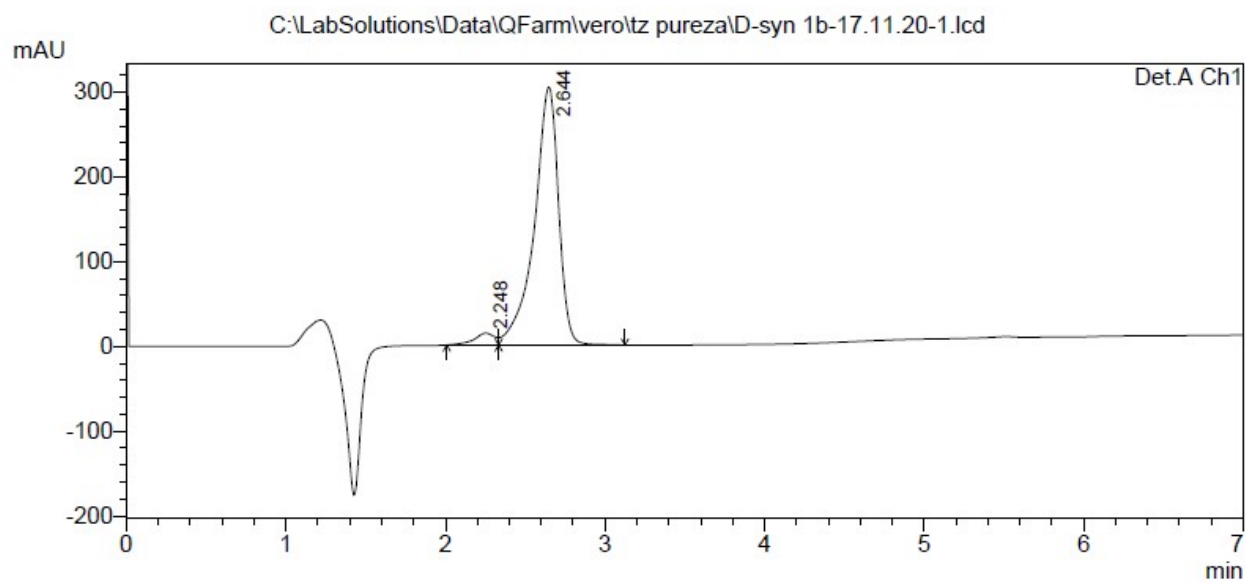


Figure S21: Chromatogram of compound D-syn-1b, monitored at 215 nm

## Experimental Methods

### Chemical Stability of D-anti-1b

A stock solution of D-anti-1b (0.194 mg/mL in MeCN) was prepared. A 500  $\mu$ L aliquot of stock solution was added to PBS buffer (pH 7.2, 500  $\mu$ L), and the mixture was incubated at 27 °C. Aliquots of 40  $\mu$ L were taken at 30 min, 1 h, 2 hs, 4 hs, and 6 hs. The samples were immediately analysed by HPLC to quantify the thiazolidine and by-products. These analyses were conducted three times for each compound.

Quantification was carried out by HPLC. The system was composed of a Waters Alliance (Waters Corporation, MA, USA) equipped with a Waters 2695 solvent delivery module in a quaternary gradient mode and a Waters 2669 PDA detector. Analysis was carried out at 215 nm in Phenomenex Luna C18 column (4.6 mm x 150 mm, 5  $\mu$ m) at room temperature and the UV wavelength detection was 215 nm. The solvent was 99 % MeCN (0.05 % Formic acid) as mobile phase A and H<sub>2</sub>O (0.05 % Formic acid) as mobile phase B at a flow rate of 1 mL/min. The gradient program was as follows: 50-99 % A (0-10 min), 99 % A (10-12 min) and 50 % A (12.01-15 min). Calibration standards of D-anti-1b were prepared at concentrations of 0.039, 0.097, 0.155, 0.194, 0.233 mg/mL from a standard solution of 1 mg/mL by appropriate dilution with acetonitrile. An aliquot of 20  $\mu$ L of this solution was injected for the HPLC analysis.

### LCMS/MS chromatogram

For the chromatogram on LCMS of D-anti-1b the following conditions were employed. Column Evo C18 5u, 4,6 x150 mm. A: formic acid 0,1 %. B: formic acid 0,1 % in MeCN. Flow 1.25 mL/min; split for ESI 1:4, gradient TO B conc = 50 %, T10 B conc= 98 %, conditions ESI: Interface voltage -4,5 kV / nebulizing gas flow 3 L/min, DL Temp 250 °C, heat block temp 400 °C, drying gas flow 15 L/min, acquisition range 100-1000 Da. A Shimadzu 8040 equipment was employed.

### Protein preparation for $K_i$ determinations

The mature form of NDM-1 and VIM-2 were cloned in a modified version of the pET28b+(TEV),<sup>6</sup> with the TEV cleavage site instead of the corresponding to trombine, and pET28b+, respectively. The N-terminal His<sub>6</sub>-MBLs were express on *E. coli* BL21(DE3) and induced with 0.2 mM IPTG and 0.5 mM ZnSO<sub>4</sub> for 16 hs at 18 °C. The cells were disrupt by sonication and the crude extract was loaded on a Ni-Sepharose column, the obtained fusion proteins were cut with TEV (NDM-1) or thrombin (VIM-2) proteases

To purify IMP-1 the plasmid pET26-*bla*IMP-1 was employed. The MBL was expressed in *E. coli* BL21(DE3) with 0.5 mM IPTG and 0.5 mM ZnSO<sub>4</sub> for 16 hs at 20 °C. The cell lysis was performed by sonication and the soluble fraction was dialyzed for 16 hs against 50 mM Tris-Cl pH 7.5, 100 mM ZnSO<sub>4</sub> and 10 mM  $\beta$ -mercaptoethanol and then clarified by centrifugation. This fraction was loaded on a cationic exchange equilibrated column with 50 mM Tris-Cl pH 7.5, IMP-1 was eluted with 0-500 mM NaCl gradient in 50 mM Tris-Cl pH 7.5.

All protein preparations have a purity >95%, as determined by SDS-PAGE.

### Determination of the $K_i$ .

Imipenem hydrolysis by the MBLs was monitored following the changes in absorbance at 300 nm using a  $\Delta\epsilon_{300} = -9000 \text{ M}^{-1} \text{ cm}^{-1}$  (JascoV-670 spectrophotometer). Reactions were carried out in 0.1 cm path length quartz cuvettes with a final enzyme concentration of 1 nM (NDM-1) and 3 nM (IMP-1 and VIM-2) in 10 mM HEPES pH 7.5, 200 mM NaCl, 50 mg/L BSA and 20  $\mu$ M ZnSO<sub>4</sub> at 30 °C. Thiazolidines were dissolved in DMSO to a final concentration of 100 mM and diluted in the reaction buffer to the desired concentration. The reactions were initiated with enzyme addition to a substrate and inhibitor mixture. Linear initial phase of the time courses was observed for all the conditions; in presence of the inhibitor a decreased hydrolysis rate was measured with respect to the reaction in its absence. The inhibition constants ( $K_i$ ) were determined by data fitting to the Competitive Inhibition Model implemented in GraphPad Prism 5.0.

## Bacterial cell preparations for inhibition studies

*E. coli* cells carrying the pMBLe or pMBLe-NDM-1 vector<sup>7</sup> were inoculated in 10 mL of LB media supplemented with 25 mg/L gentamicin and were grown at 37 °C until cells reached an OD<sub>600</sub> of 0.6. For NDM-1 induction, 100 µM IPTG was added and the culture was incubated for another 2 hs at the same temperature. The cells were pellet by centrifugation and resuspended 1 mL of 50 mM sodium phosphate pH 7.0 with 5 µM ZnSO<sub>4</sub>. This process was repeated 3 times; finally, the cells were resuspended in the same buffer at an OD<sub>600</sub> of 0.15. For the NMR experiments, to 500 µL of the cell suspension (with 10 % D<sub>2</sub>O) different concentrations of each compound and/or 500 µM imipenem were added and placed in the NMR tube for data acquisition. Supernatants from the cell suspensions were collected by centrifugation and then filtered through 0.22 µm filters for the controls.

## <sup>1</sup>H NMR measurements and analyses

All spectra were acquired on a Bruker Avance 600 MHz spectrometer equipped with a TXI probe. All experiments were done at 25 °C and acquired with 64 scans and 32K data points using standard techniques. NMR spectra were processed and analysed with TopSpin 3.2 (Bruker). All spectra in a given series were plotted at the same scaling ratio.

## *In-cell* IC<sub>50</sub> measurements and analyses

For the estimation of the *In-cell* IC<sub>50</sub> we followed the procedure already reported.<sup>8,9</sup> *E. coli* cells expressing NDM-1, anchored to the outer membrane, were exposed to imipenem and after 9 to 15 min the antibiotic was completely degraded. In the presence of the inhibitor this hydrolysis rate was slower. After 30 min of incubation in the magnet, *E. coli* cell were still viable (Figure S13). We also confirmed that imipenem is stable in the employed buffer and in the presence of *E. coli* cells lacking the carbapenemases (Figure S14). Cell lysis leading to NDM-1 leakage into the medium was not observed, confirming that the reaction occurred within the bacterial periplasm (Figure S14).

In order to evaluate the potency of the inhibitors in bacterial cells, we calculate the percentage of inhibition 15 min after the initiation of the reaction employing the following equation (Equation 1),

$$\%_{\text{inhibition}} = 100 - 100 \times \frac{S_T - S_1}{S_T - S_2} \quad (\text{Equation 1})$$

where [S<sub>1</sub>] and [S<sub>2</sub>] correspond to the substrate concentration, in the presence and absence of inhibitor, respectively, and are obtained by the integral of the signal between 1.22-1.18 ppm. [S<sub>T</sub>] is the sum of [S<sub>2</sub>] and [P<sub>2</sub>] or [S<sub>1</sub>] and [P<sub>1</sub>], where [P<sub>1</sub>] and [P<sub>2</sub>] are product concentration obtained by the integrals of signals at 1.17-1.12 ppm in the presence and absence of the inhibitor, respectively. IC<sub>50</sub> values are obtained by fitting the %<sub>inhibition</sub> vs. inhibitor concentration to Equation 2:

$$\%_{\text{inhibition}} = 100 - \frac{100}{1 + \left(\frac{[I]}{IC_{50}}\right)^n} \quad (\text{Equation 2})$$

where [I] is the inhibitor concentration and *n* is the cooperativity factor.

## Antimicrobial susceptibility testing

Eight clinical isolates of different species within the Enterobacterales order, expressing NDM, VIM or IMP MBLs, were used in these experiments. MICs were determined by the broth microdilution method according to the guidelines of the Clinical and Laboratory Standards Institute (CLSI).<sup>10</sup> Serial doubling dilutions of imipenem (imipenem-cilastatin, Merck & CO, Whitehouse Station, NJ, USA) and meropenem (Zuventus Healthcare Ltd., Bari-Brahmana, Jammu, India) from 64 mg/L to 0.03 mg/L were prepared, while the MMTZs were tested at a constant concentration of 100 mg/L. Results presented are the mode of three biological replicates.

## Cell Culture and Survival Assay

The Vero (African green monkey kidney), HEK293 (human embryonic kidney) and L929 (mouse fibroblast) cell lines were cultured in Dulbecco's modified Eagle's medium (DMEM, Gibco) supplemented with 10 % fetal bovine serum, penicillin G (100 units/mL, Sigma), and streptomycin (100 mg/L, Sigma) and maintained in a 5 % CO<sub>2</sub> humidified incubator at 37 °C. Cell viability was analysed using the MTT assay.<sup>11</sup> Briefly, cells were seeded in 96-well plates at a density of 4500 cells per well. The synthesized compounds were dissolved in DMSO (Merck) at 114.6 mM and then diluted in culture medium to achieve the final concentration for the different treatments. As negative controls, cells were incubated with the corresponding concentration of DMSO (Merck), according to the dilution. After 24 hs of treatment, cells were stained with 3-(4,5-dimethyl-2-thiazolyl)-2,5-diphenyl-2H-tetrazolium bromide (MTT) (0.5 mg/mL; Sigma) for 4 hs at 37 °C. After the removal of the culture medium, formazan crystals were dissolved in DMSO and the absorbance was measured at 562 nm using a microplate reader.

## Crystallization and Structure Determination

For crystallographic studies, recombinant forms of NDM-1, VIM-2 and IMP-1 were produced as previously described.<sup>2,12,13</sup> IMP-1 and NDM-1 were crystallized as previously.<sup>2,12</sup> VIM-2 was crystallized at 19 °C by mixing 1 µL protein (8 mg/mL in 50 mM HEPES pH 7.5, 100 mM NaCl, 1 mM TCEP and 0.1 mM ZnCl<sub>2</sub>) with 2 µL crystallization reagent (0.1 M Mg(HCO<sub>3</sub>)<sub>2</sub>, 25 % PEG 3350) and equilibrated against 500 µL crystallization reagent. NDM-1 complexes were obtained by soaking crystals in 2 mM inhibitor (dissolved in crystallization reagent) added directly to the drop for 90 min (L-*anti-1b*) or 120 min (D-*syn-1b*); crystals were then cryo-protected by brief exposure to 20 % (v/v) aqueous glycerol (in well solution) and subsequently flash-cooled in liquid nitrogen. IMP-1 and VIM-2 complexes were obtained by soaking crystals in cryo-protectant (well solution diluted to 25 % (v/v) aqueous glycerol) supplemented with 4 mM inhibitor for 60 min; crystals were subsequently flash-cooled in liquid nitrogen.

Diffraction data were collected at 100 K at Diamond Light Source on beamlines I04 (IMP-1:D-*syn-1b*), I04-1 (IMP-1:L-*anti-1b*; VIM-2:L-*anti-1b*; VIM-2:D-*syn-1b*) or I03 (NDM-1:L-*anti-1b*; NDM-1:D-*syn-1b*). IMP-1:L-*anti-1b*, IMP-1:D-*syn-1b* and NDM-1:L-*anti-1b* data were integrated in DIALS<sup>14</sup> and scaled and merged in Aimless (CCP4 suite<sup>15</sup>); VIM-2:L-*anti-1b* data were integrated in iMosflm<sup>16</sup> and scaled and merged in Aimless; VIM-2:D-*syn-1b* and NDM-1:D-*syn-1b* data were integrated in XDS<sup>17</sup> and scaled and merged in XSCALE as part of the xia2 pipeline<sup>18</sup>. Phases were calculated by molecular replacement in Phaser<sup>19</sup>, using PDB IDs 4bz3<sup>1</sup> (VIM-2), 6rmf<sup>12</sup> (NDM-1) or 5hh4<sup>20</sup> (IMP-1). Structures were completed by iterative rounds of manual model building in Coot<sup>21</sup> and refinement in Phenix<sup>22</sup>. VIM-2:L-*anti-1b* data were twinned as determined by Xtriage (h, -k, -l; 0.15 twin fraction). Ligand structures and geometric restraints were calculated with Phenix eLBOW<sup>22</sup>. Structure validation was assisted by Molprobit<sup>23</sup> and Phenix. Figures were created in PyMol ([www.pymol.org](http://www.pymol.org)).

## QM-MM calculations

For hybrid Quantum Mechanics-Molecular Mechanics (QM-MM) calculations, we used Self-Consistent Charge Density Functional Tight Binding (SCC-DFTB)<sup>24</sup> to describe the QM region and the ff14SB force field<sup>25</sup> to describe the MM region as implemented in Amber16<sup>26,27</sup>.

The initial structures were taken from the crystal structures of NDM-1 in complex with L-*anti-1b* and D-*syn-1b*, and built *in-silico* for the oxazolidine analogs by replacing the sulphur atom with an oxygen. Hydrogen atoms were added, and each protein was immersed in a truncated octahedral periodic box with a minimum solute-wall distance of 8 Å, filled with explicit TIP3P water molecules<sup>28</sup>, using the AMBER16 leap module<sup>27</sup>. The van der Waals radius, force constants and equilibrium distances, angles and dihedral for L-*anti-1b* and D-*syn-1b* were taken from gaff database and partial charges were RESP charges computed using Hartree-Fock method and 6-31G\* basis set<sup>27,29</sup>. To accommodate solvent molecules and possible clashes, an initial minimization at the molecular mechanic level of each complex structure was performed, followed by QM-MM geometry optimization. The QM region consisted of both Zn(II) ions plus the coordinated side chains of residues Trp87, His116, His118, Asp120, His196, Cys221, Asn233, His263, and the L-*anti-1b* or D-*syn-1b* compound.



## References

- 1 J. Brem, S. S. Van Berkel, D. Zollman, S. Y. Lee, O. Gileadi, P. J. McHugh, T. R. Walsh, M. A. McDonough and C. J. Schofield, *Antimicrob. Agents Chemother.*, 2016, **60**, 142–150.
- 2 P. Hinchliffe, M. M. González, M. F. Mojica, J. M. González, V. Castillo, C. Saiz, M. Kosmopoulou, C. L. Tooke, L. I. Llarrull, G. Mahler, R. A. Bonomo, A. J. Vila and J. Spencer, *Proc. Natl. Acad. Sci.*, 2016, **113**, E3745–E3754.
- 3 H. Zhang, G. Ma, Y. Zhu, L. Zeng, A. Ahmad, C. Wang, B. Pang, H. Fang, L. Zhao and Q. Hao, *Antimicrob. Agents Chemother.*, 2018, **62**, e01579-18.
- 4 J. E. Raczynska, I. G. Shabalin, W. Minor, A. Wlodawer and M. Jaskolski, *Drug Resist. Updat.*, 2018, **40**, 1–12.
- 5 H. Feng, X. Liu, S. Wang, J. Fleming, D. C. Wang and W. Liu, *Nat. Commun.*, 2017, **8**, 2242–2242.
- 6 M. M. González, M. Kosmopoulou, M. F. Mojica, V. Castillo, P. Hinchliffe, I. Pettinati, J. Brem, C. J. Schofield, G. Mahler, R. A. Bonomo, L. I. Llarrull, J. Spencer and A. J. Vila, *ACS Infect. Dis.*, 2016, **1**, 544–554.
- 7 L. J. Gonzalez, G. Bahr, T. G. Nakashige, E. M. Nolan, R. A. Bonomo, A. J. Vila, L. J. González, G. Bahr, T. G. Nakashige, E. M. Nolan, R. A. Bonomo and A. J. Vila, *Nat Chem Biol*, 2016, **12**, 516–522.
- 8 C. Dalvit, E. Ardin, G. P. Fogliatto, N. Mongelli and M. Veronesi, *Drug Discov. Today*, 2004, **9**, 595–602.
- 9 J. Ma, S. McLeod, K. MacCormack, S. Sriram, N. Gao, A. L. Breeze and J. Hu, *Angew Chem Int Ed Engl*, 2014, **53**, 2130–2133.
- 10 CLSI, *Performance Standards for Antimicrobial Susceptibility Testing Performance Standards for Antimicrobial Susceptibility Testing*, Wayne, PA: Clinical and Laboratory Standards Institute, 2019, vol. 29th ed.
- 11 T. Mosmann, *J. Immunol. Methods*, 1983, **65**, 55–63.
- 12 A. Krajnc, J. Rgen Brem, P. Hinchliffe, K. Calvopiñ, T. D. Panduwawala, P. A. Lang, J. J. A. G. Kamps, J. M. Tyrrell, E. Widlake, B. G. Saward, T. R. Walsh, J. Spencer and C. J. Schofield, *J Med Chem*, 2019, **26**, 8544–8556.
- 13 S. S. Van Berkel, J. Brem, A. M. Rydzik, R. Salimraj, R. Cain, A. Verma, R. J. Owens, C. W. G. Fishwick, J. Spencer and C. J. Schofield, *J. Med. Chem.*, 2013, **56**, 6945–6953.
- 14 G. Winter, D. G. Waterman, J. M. Parkhurst, A. S. Brewster, R. J. Gildea, M. Gerstel, L. Fuentes-Montero, M. Vollmar, T. Michels-Clark, I. D. Young, N. K. Sauter and G. Evans, *Acta Crystallogr. Sect. D Struct. Biol.*, 2018, **74**, 85–97.
- 15 N. 4 Collaborative Computational Project, *Acta Crystallogr. Sect. D Biol. Crystallogr.*, 1994, **50**, 760–763.
- 16 T. G. G. Battye, L. Kontogiannis, O. Johnson, H. R. Powell and A. G. W. Leslie, *Acta Crystallogr. Sect. D Biol. Crystallogr.*, 2011, **67**, 271–281.
- 17 W. Kabsch, B. A. T., D. K., K. P. A., D. K., M. S., R. R. B. G., E. P., F. S., W. K., K. W., K. W., K. W., K. W., K. P. and W. M. S., *Acta Crystallogr D Biol Crystallogr*, 2010, **66**, 125–132.
- 18 G. Winter, C. M. C. Loblely and S. M. Prince, *Acta Crystallogr. Sect. D Biol. Crystallogr.*, 2013, **69**, 1260–1273.
- 19 A. J. McCoy, R. W. Grosse-Kunstleve, P. D. Adams, M. D. Winn, L. C. Storoni and R. J. Read, *J. Appl. Crystallogr.*, 2007, **40**, 658–674.
- 20 M. F. Mojica, S. G. Mahler, C. R. Bethel, M. A. Taracila, M. Kosmopoulou, K. M. Papp-Wallace, L. I. Llarrull, B. M. Wilson, S. H. Marshall, C. J. Wallace, M. V. Villegas, M. E. Harris, A. J. Vila, J. Spencer and R. A. Bonomo, *Biochemistry*, 2015, **54**, 3183–3196.
- 21 P. Emsley and K. Cowtan, *Acta Crystallogr. Sect. D Biol. Crystallogr.*, 2004, **60**, 2126–2132.
- 22 P. D. Adams, P. V. Afonine, G. Bunkóczi, V. B. Chen, I. W. Davis, N. Echols, J. J. Headd, L. W. Hung, G. J. Kapral, R. W. Grosse-Kunstleve, A. J. McCoy, N. W. Moriarty, R. Oeffner, R. J. Read, D. C. Richardson, J. S. Richardson, T. C. Terwilliger and P. H. Zwart, *Acta Crystallogr. Sect. D Biol. Crystallogr.*, 2010, **66**, 213–221.
- 23 V. B. Chen, W. B. Arendall, J. J. Headd, D. A. Keedy, R. M. Immormino, G. J. Kapral, L. W. Murray, J. S. Richardson and D. C. Richardson, *Acta Crystallogr. Sect. D Biol. Crystallogr.*, 2010, **66**, 12–21.
- 24 M. Gaus, Q. Cui and M. Elstner, *J. Chem. Theory Comput.*, 2011, **7**, 931–948.
- 25 J. A. Maier, C. Martinez, K. Kasavajhala, L. Wickstrom, K. E. Hauser and C. Simmerling, *J. Chem. Theory Comput.*, 2015, **11**, 3696–3713.
- 26 G. D. M. Seabra, R. C. Walker, M. Elstner, D. A. Case and A. E. Roitberg, in *Journal of Physical Chemistry A*, 2007, vol. 111, pp. 5655–5664.

- 27 H. G. D.A. Case, R.M. Betz, D.S. Cerutti, T.E. Cheatham, III, T.A. Darden, R.E. Duke, T.J. Giese, C. A.W. Goetz, N. Homeyer, S. Izadi, P. Janowski, J. Kaus, A. Kovalenko, T.S. Lee, S. LeGrand, P. Li, I. Lin, T. Luchko, R. Luo, B. Madej, D. Mermelstein, K.M. Merz, G. Monard, H. Nguyen, H.T. Nguyen, J. S. Omelyan, A. Onufriev, D.R. Roe, A. Roitberg, C. Sagui, C.L. Simmerling, W.M. Botello-Smith and L. X. and P. A. K. R.C. Walker, J. Wang, R.M. Wolf, X. Wu, .
- 28 W. L. Jorgensen, J. Chandrasekhar, J. D. Madura, R. W. Impey and M. L. Klein, *J. Chem. Phys.*, 1983, **79**, 926–935.
- 29 C. I. Bayly, P. Cieplak, W. Cornell and P. A. Kollman, *J. Phys. Chem.*, 1993, **97**, 10269–10280.